J. Fluid Mech. (1985), *vol.* 154, *pp.* 63–90
Printed in Great Britain

Attached cavitation and the boundary layer: experimental investigation and numerical treatment

By J. P. FRANC AND J. M. MICHEL
Institut de Mécanique de Grenoble, Université de Grenoble,
B.P. 68, 38402 Saint-Martin-d'Hères, France

(Received 12 June 1984)

Attached cavitation on a wall with continuous curvature is investigated on the basis of experiments carried out on various bodies (circular and elliptic cylinders, NACA 16 012 foil). Visualization of the boundary layer by dye injection at the leading edge shows that a strong interaction exists between attached cavitation and the boundary layer. In particular, it is shown that the cavity does not detach from the body at the minimum pressure point, but behind a laminar separation, even in largely developed cavitating flow. A detachment criterion which takes into account this link between attached cavitation and boundary layer is proposed. It consists of connecting a cavitating potential-flow calculation and a boundary-layer calculation. Among all the theoretically possible detachment points, the actual detachment point is chosen to be the one for which the complete calculation predicts a laminar separation just upstream. This criterion, applied to the NACA foil, leads to a prediction which is in good agreement with experimental results.

1. Introduction

The present study is related to liquid flow under developed cavitation conditions, with a cavity attached to a wall of regular geometry. In such a case, the cavitation forms a continuous and steady pocket over an area of size comparable to a significant dimension of the wall. A key question is raised when facing this phenomenon: how is the position of cavity detachment determined? (the term 'detachment' is used here in order to avoid any confusion with the term 'separation' generally reserved for the boundary layer). The answer to this question has a direct bearing on the numerical solution to the problem – since the boundary conditions are different on either side of the detachment – and on the prediction of the forces acting on the wall under attached cavitation conditions.

A well-established fact can be used as a guideline: in incipient cavitation, there is a direct link between separation of the laminar boundary layer (when it exists) and the initial signs of cavitation, either sheet cavitation or bubble-band cavitation, both of which are located in the recirculation zone downstream of the detachment. This link was proposed by Alexander as early as 1968 in order to explain the difference between the absolute value of the minimum pressure coefficient on the wall and the value of incipient cavitation number σ_{vi}. It was demonstrated using optical means – schlieren method or holographic method – by Arakeri & Acosta (1973) and Arakeri (1975), and more recently by Van der Meulen (1978, 1980). It implies that, before reaching the cavitating zone, the liquid particles pass through a region where the pressure is less than the vapour pressure, and in fact becomes a tension. The capacity of a liquid to withstand tension was demonstrated a long time ago by laboratory experiments (Knapp, Daily & Hammitt 1970). It can also be found in industrial situations if the liquid has few air nuclei, especially large-size nuclei, i.e. with radius exceeding about five micrometres in the case of water: this was shown as early as 1972, as reported by Le Goff & Lecoffre (1982). It may be noted that, if the cavitating zone was the minimum-pressure zone, the longitudinal pressure gradient $\partial p/\partial s$ upstream of the cavitation would be negative throughout and laminar separation could not then take place.

The case of detachment under developed cavitation or supercavitation conditions is not so clear and has not been systematically studied to date. The only experimental data available concern spheres and cylinders (Brennen 1970; Oba, Ikohagi & Yasu 1980). They show that the detachment position depends on the external flow velocity when the cavitation number is kept constant, and thus when the overall flow geometry, especially cavity length, does not vary to any great extent. Such dependence cannot be explained only by the behaviour of the laminar boundary layer upstream of the cavity since the streamwise characteristics of the laminar boundary layer do not depend on Reynolds number (Schlichting 1960). This is why Arakeri (1975) in his simplified representation of the flow introduces a small zone located between the laminar separation and the cavity detachment. In this zone, the liquid inertia has negligible influence and the predominant forces are surface tension and viscosity. Arakeri proposes an empirical method for cavity detachment calculation based on his own observations in axisymmetric flow. The final expression for detachment position includes a term describing the movement of laminar separation under the effect of cavitation, and a term relating to variations in distance between separation and detachment. This latter term accounts for local effects, and the external velocity U appears in the momentum thickness of the boundary layer at separation and also in the Taylor–Saffman number $\mu U/T$, where μ and T are the viscosity and surface tension of the liquid respectively. Arakeri's method predicts the correct detachment variations in relation to flow velocity in the case of a circular cylinder with, however, a deviation of some 20° with respect to our experimental results. Owing to the lack of available data, the method has been tested to date only on cylindrical and spherical bodies.

The aim of the present article is to obtain an overall view of the mechanisms governing the detachment of largely developed cavities from solid walls with continuous curvature, by examining a sufficiently wide variety of configurations. In this respect, a two-dimensional flow around plane foils offers the advantage of producing considerable variations in longitudinal pressure gradient simply by changing the angle of attack. The phenomena are easier to observe if use is made of bodies giving a moderate pressure gradient at small angle of attack and, at higher angles of attack, producing underpressures which are not too deep and not too close to the leading edge. In view of these two requirements, the first choice was elliptical cylinders with a minor-to-major axis ratio of 1:4 and 1:8, although consideration was also given to flow around a cylinder with circular section. In a second stage, a NACA 16 012 symmetrical hydrofoil, already used by Van der Meulen (1980), was studied in depth for a wide range of angles of attack. For the second elliptical cylinder foil and NACA foil, a simple flow-visualization method was used to locate the laminar separation point of the boundary layer and the transition to turbulent conditions. The overall results show that the dependence of detachment position on external flow velocity reduces and tends to disappear as the thickness of the foil body is decreased: this tendency reduces the local effect of interfacial and viscous forces for thin bodies to a minor role. If they are completely ignored, the problem of cavity detachment is reduced to the problem of interaction between the largely developed cavitation and the boundary layer before it on the wall. By this important simplification, it is possible to apply the method used in aerodynamics to the cavitating flows, which consists of calculating the external potential flow first and then the boundary layer determined by this flow. The aim is to give a practical description of the coexistence of cavitation and the boundary layer, the former depending on the general pressure level at a given velocity, while the latter is controlled mainly by the pressure gradient. This approach considers cavitation to be an established phenomenon imposing its own conditions on the boundaries, and not as the disturbance of a non-cavitating reference flow.

Despite the fact that local flow representation difficulties still remain, as described below, when the experimental position of the detachment is introduced in the first phase of the calculation, the method gives the laminar separation as the result of the second phase approximately in the same position as that found in the experiment and for the same conditions of existence. Moreover, when the procedure is repeated, the detachment position can be predicted from a process shown to be convergent by the numerical experiment. This was verified not only for small and large angles of attack, where detachment is preceded by laminar separation, but also for medium angles of attack where the natural transition to turbulence may prevent cavitation from occurring when ambient pressure is not sufficiently low. The results obtained for thin bodies would therefore seem to justify both the assumption made and the method chosen.

The experimental procedures and numerical methods used are described in §§2 and 3. In §4, the preliminary results obtained during the first research stage are given. Section 5 concerns the experimental results obtained with the NACA 16 012 hydrofoil. The methods developed during the first stage have been used to the full. Charts of various flow regimes were drawn up for a range of angle of attack values and cavitation numbers. Several cavitation figures presented here have never been observed previously. In addition, certain curious facts related to the interaction between cavitation and the boundary layer would not seem to have been indicated in the past. In the final section of this article, the results of numerical calculations on the NACA foil are analysed. Owing to the lack of an available model for partial cavities closing over the body, it was not possible to calculate the external potential flow by nonlinear methods for any other case than non-cavitating or supercavitating flows. From the overall results, however, a predictive method can be built to give the detachment position. This is compared with the results obtained using the Arakeri method.

A special point needs to be made here: the experimental results were obtained in a hydrodynamic tunnel characterized by the high level of deaeration imposed on the water. As a result, the air nuclei content in the water is very small and developed transient-bubble cavitation does not occur. Under present experimental conditions, the only type of developed cavitation that can be produced in the tunnel is cavitation attached to a wall. This is a favourable factor for studies of boundary-layer/cavitation interaction and helps avoid any confusion between the effect of air nuclei and the effect of the boundary layer on attached cavitation. On the other hand, this condition may impose limits to the possible application of the results presented here on a much larger geometric scale. For example, recent results on separated transient bubble cavitation (Le Goff & Lecoffre 1982) show that cavitating flows of this type, on both models and prototypes of geometric ratio λ, cannot be geometrically similar unless the ratio of air nuclei content is of the order of $1/\lambda^3$. Despite the fact that this condition is not, theoretically, sufficient to meet the explosion conditions of each of

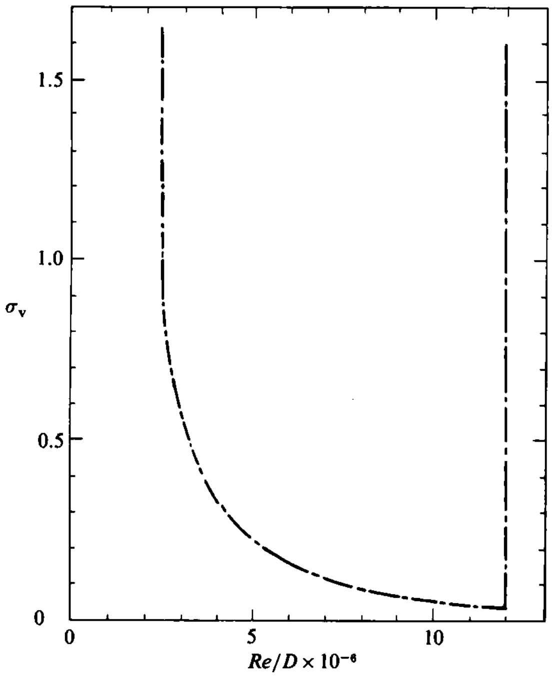

FIGURE 1. Possible range of σ_v values versus Re/D.

the bubbles, it would nevertheless appear in practice to provide similitude of forces on the bodies. This means that the flow around the large prototype must contain a much smaller number of nuclei per unit volume of liquid than the flow around the small model. In order to transpose the method proposed here to larger scales, it must be assumed that cavitation is also of the attached type in the large-scale case. At the present time, the exact conditions governing formation of either type of cavitation are not known. The point is made only to clarify the problem and the conditions of validity of the results obtained.

2. Experimental setup and methods

The tests were carried out in the second free-surface channel of the hydrodynamic tunnel at Grenoble University (Dodu, Duport & Michel 1968). The test section is 1.6 m long, 0.12 m wide and 0.40 m high. The absolute pressure p_0 at the free surface of the channel can be fixed between a value close to the vapour pressure p_v and atmospheric pressure, while the free-stream velocity U is in the range 2.5–13.0 m/s. Thus, the Reynolds number $Re = \rho UD/\mu$ where ρ is the specific mass of water, is in the range 25000–130000 for a characteristic size D = 1 cm. The cavitation index σ_v, which is defined as $\sigma_v = 2(p_0+\rho gh-p_v)/\rho U^2$ where g is the acceleration due to gravity and h the submersion depth of the body, can be reduced to 0.03. Figure 1 gives the possible values of σ_v versus the values of $\rho U/\mu = Re/D$ m^{-1}. When largely developed cavities are present, the dynamic similarity parameter is the relative underpressure $\sigma = 2(p_0+\rho gh-p_c)/\rho U^2$, where p_c is the absolute pressure inside the cavity. In operations with supercavitating flows, p_c-p_v is found to be of the order of 1 mm of mercury, i.e. about 100 or 200 Pa. This value is small with respect to the pressure difference which defines σ_v, so that σ is taken equal to σ_v. All the measuring devices are of standard use in hydrodynamic laboratories and allow σ_v and *Re* to be determined with a relative error of about 1 %.

The mean velocity profile is constant over the channel width except on the 1.5 cm thick boundary layers adjacent to the vertical walls. The flow can therefore be considered two-dimensional in the median part of the channel, i.e. over a width of about 9 cm. In this area, the turbulence rate $Tu = (\overline{u'^2})^{\frac{1}{2}}/U$ measured by a hot-film anemometer, varies from 0.12–0.16 % when the velocity U varies from 3 to 12 m/s. The photographs in figure 18 show that the two-dimensional nature of cavity detachment is not necessarily affected by the boundary layers of the wall at the tips of the foil. They also show that interference cavitation may occur on the sides of the channel. This cavitation, which appears to be connected with the locally three-dimensional boundary layer and its streamwise velocity, has not been studied further.

The air nuclei content of water is estimated by means of a Venturi device (Oldenziel 1982) in which the nuclei with critical pressure higher than the throat pressure explode and can then be counted by the noise emitted during implosion. Under the operating conditions of the hydrodynamic tunnel, the average number of air nuclei of critical pressure greater than -0.35×10^5 Pa is very small (between 0.05 and 0.3 per cm^3). Such nuclei can also sustain negative pressures on the foils, taking into account the time required for their explosion. Figure 19(*b*), shows, however, that the explosion of a few nuclei may occur incidentally.

The four bodies were tested at the same submersion depth $h = 20$ cm, i.e. at mid-channel height. The diameter of the circular cylinder is 1 cm. The major axis of both the elliptical cylinders is $a = 4$ cm (chord 8 cm), and the minor axes are respectively $b_1 = 1$ cm and $b_2 = 0.5$ cm. The chord of the symmetrical NACA foil is $c = 10$ cm; its maximum thickness at the relative abscissa 0.5 is 1.2 cm. The bodies are made of stainless steel. Except for the circular cylinder, they are machined by milling: about two hundred passages are necessary in order to obtain a maximum distance of 2 μm between the theoretical curve and the edges of the polygonal line. The angles are then rounded by manual polishing. The roughness in the flow direction does not exceed 0.6 μm.

The hydrodynamic tunnel is equipped with a wall balance to hold the test body and to measure the forces: lift, drag and pitching moment. When significant, friction forces and buoyancy forces must be subtracted from the measurement results. In particular, the buoyancy force depends on the wetted geometry of the body. No correction is made for the effect of the boundary layer on the channel walls.

In this study, particular attention is given to the position of the cavity detachment point and to the streamwise features of the boundary layer upstream of the cavity. The detachment point was measured either from photographs or directly during the tests, using the reference marks at the end of the body (see figure 18, for example). In the case of the circular cylinder and for partially cavitating wakes, the unsteady nature of the flow made it necessary to use statistical methods: about two thousand photographs were taken and mean values were obtained from a sample of twenty-eight tests for each experimental point. In the case of supercavitating flows, the upper and lower parts of the flow do not interact, and the detachment point can be considered as stable in most situations. This is also true for slender bodies, even when they are followed by a short vapour cavity, provided it starts from the detachment points located on the upper and the lower side of the foil. Here, only the upper detachment point is considered.

To visualize the boundary layer, a rather simple technique was found to be suitable, although velocities were much larger than in the original case (Werlé 1980): a thin thread of water coloured with fluorescein is injected at the leading edge near the stagnation point through a small hole (0.2 mm in diameter). In practice, if the discharge of coloured water is properly adjusted, the main flow is not disturbed. The separation point of the laminar boundary layer then becomes apparent, this being promoted by the mirror effect of the body wall (figure 2, plate 1). When transition to turbulence occurs on the foil, it appears as a well-defined point under flash lighting. The transition region could probably be outlined by the repetition of such photographs, but this was outside our scope and was not undertaken. Figure 2 (*a–f*) illustrates some known features of the boundary layer in non-cavitating flow: when the angle of attack increases, laminar separation appears at the rear of the foil ($\alpha = 0°$), then moves upstream and is eliminated by transition to turbulence ($\alpha = 3°$ and 4°). Finally, it reappears near the leading edge and seems to be followed by a small recirculating bubble before the boundary layer becomes turbulent and fully separated for angles of attack close to 10°, in the case of the NACA foil, and for the Reynolds number considered. These figures have to be considered as references for comparison to the case of cavitating flows. Also, the experimental study of non-cavitating flow is useful for checking the validity of boundary-layer calculations. It must be noted that similar behaviour of the boundary layer was observed in the case of the slender elliptical cylinder.

3. Numerical approach

In both non-cavitating and supercavitating flow, the numerical approach results from the connection of two calculations: first the hydrodynamic computation of the pressure distribution on the body, given its shape and the main flow parameters; secondly the calculation of the boundary layer over the upper wetted part of the body, given the local pressure coefficients. The viscous forces are assumed not to react on the pressure distribution. Thus, the method is similar to that used in aerodynamics in its first state, but would not be applicable if large recirculating zones were present. It is suited to the case of flows with largely developed cavitation because, in actual situations, large bubbles with recirculation are not observed simultaneously with large cavities.

3.1. *Boundary-layer computations*

The boundary layer is computed by a method which was devised at ONERA (Arnal, Habiballah & Coustols 1984). Given the stagnation point and the pressure distribution over the wetted part of the foil upper side, the method describes the laminar boundary layer, the transition region and the turbulent boundary layer up to the turbulent separation point. In the laminar region, the von Kármán integral equation and the integral energy equation are used: the method proceeds step by step, and for each abscissa x gives the characteristic thickness, in particular the momentum thickness δ_2. The laminar separation is determined from a particular value of the thickness ratio $H_{32} = \delta_3/\delta_2$. The transition criterion is the Granville criterion modified first by R. Michel (1959), then by Arnal *et al.* (1984). The transition region in which intermittency appears is modelled by superimposing a turbulent flow on a laminar flow, at a rate varying with the abscissa x and determined by comparison with typical experimental results. For the fully turbulent boundary layer, the calculation uses the mixing-length concept in order to represent the Reynolds stresses through the momentum integral equation. On the whole, the method proves to work well in different situations, especially for various pressure gradients and turbulence levels.

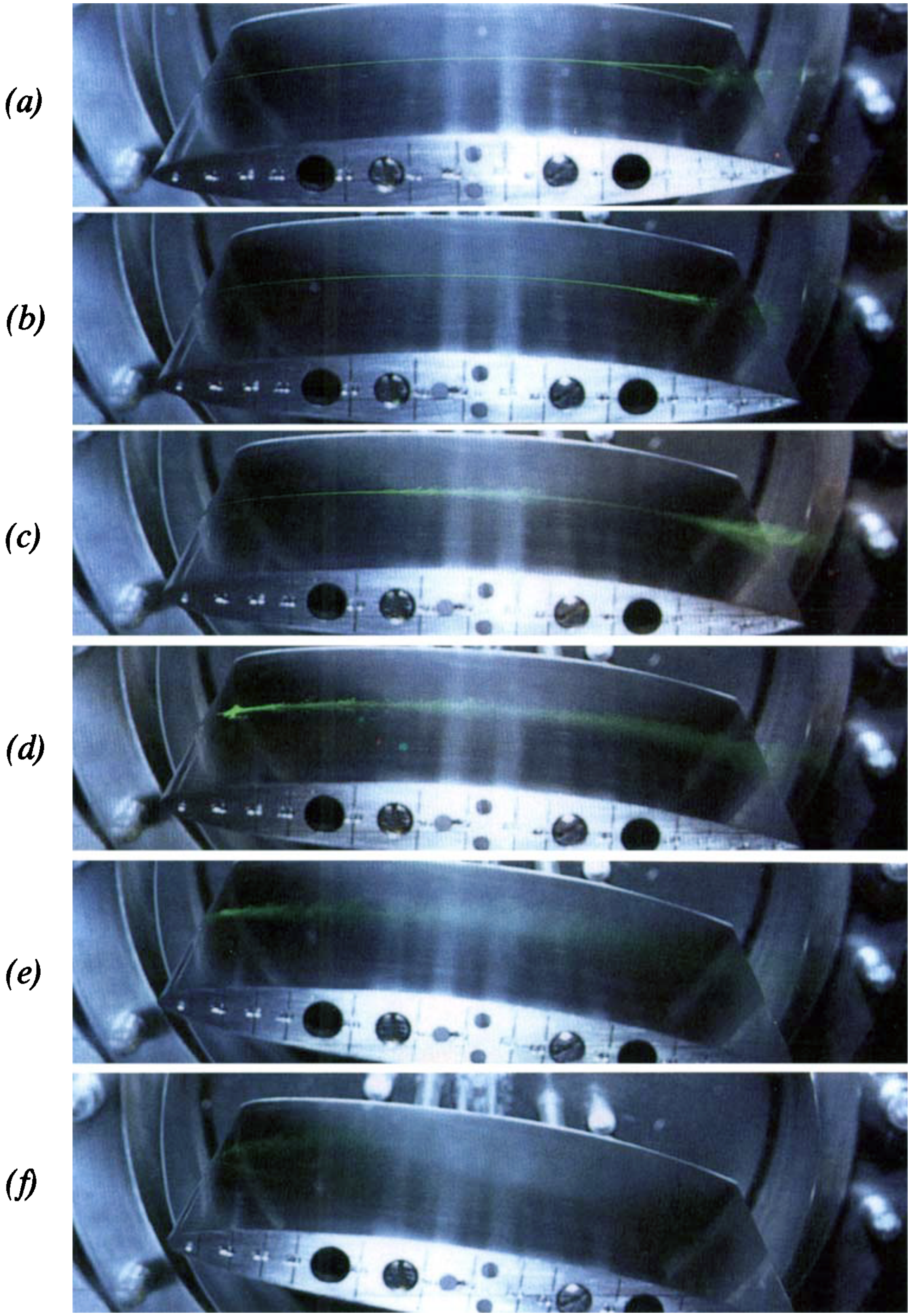

FIGURE 2. NACA 16 012; non-cavitating flow for Re = 300 000: *(a)* $\alpha = 0°$, *(b)* 3°, *(c)* 4°, *(d)* 5°, *(e)* 8°, *(f)* 10°.

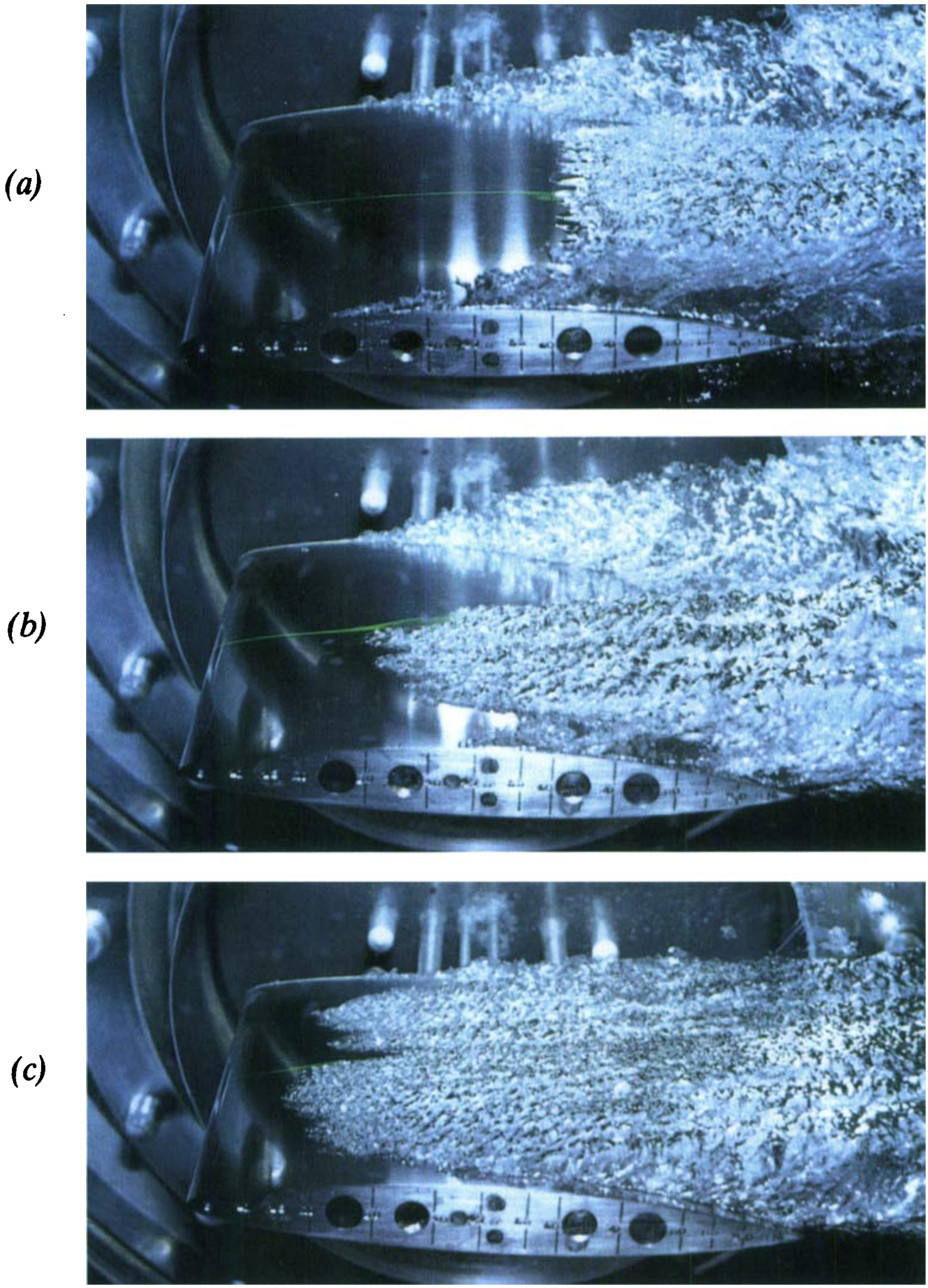

FIGURE 18. NACA 16 012; $Re = 1\,000\,000$; $\sigma_v = 0.045$: *(a)* $\alpha = 0°$, domain 1; *(b)* 3°, domain 2; *(c)* 4°, domain 2; *(d)* 5°, domain 3; *(e)* 8°, domain 3; *(f)* 15°, domain 3.

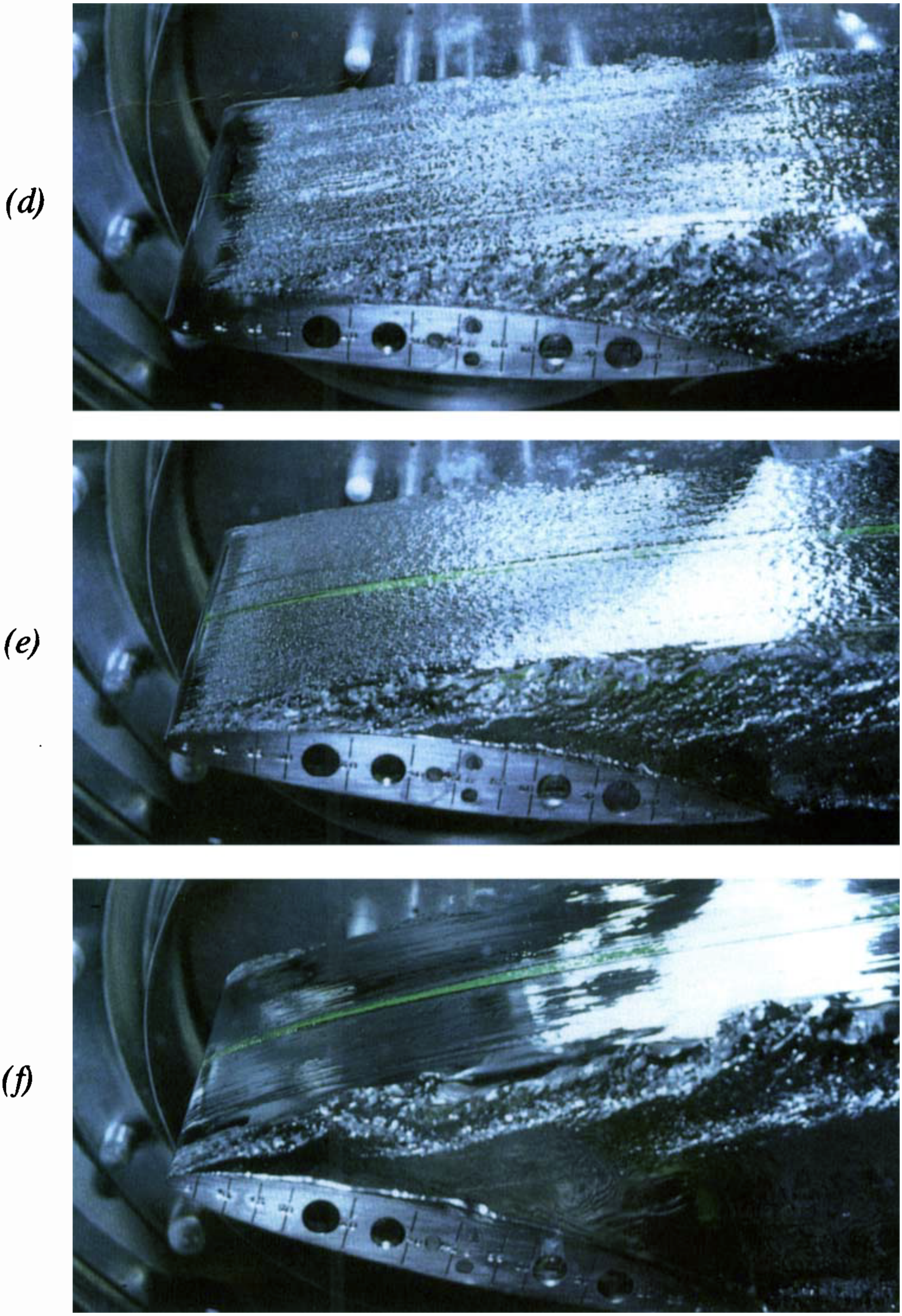

Figure 18. For legend see opposite.

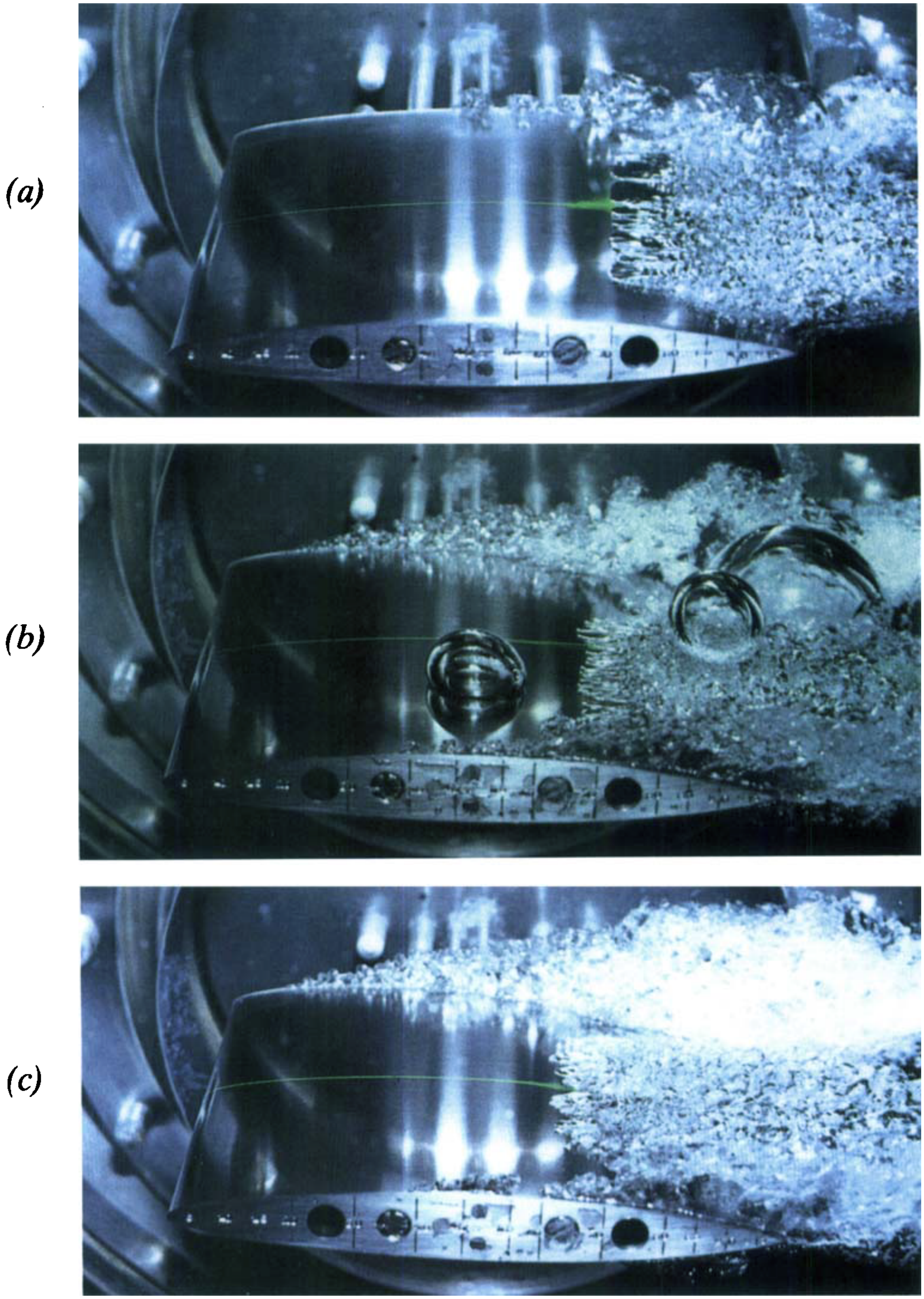

FIGURE 19. NACA 16 012; $Re = 600\,000$; $\sigma_v = 0.13$: *(a)* $\alpha = 0°$, domain 1; *(b)* 2°, domain 1; *(c)* 3°, domain 1; *(d)* 4°, non-cavitating; *(e)* 5°, domain 2; *(f)* 12°, domain 3.

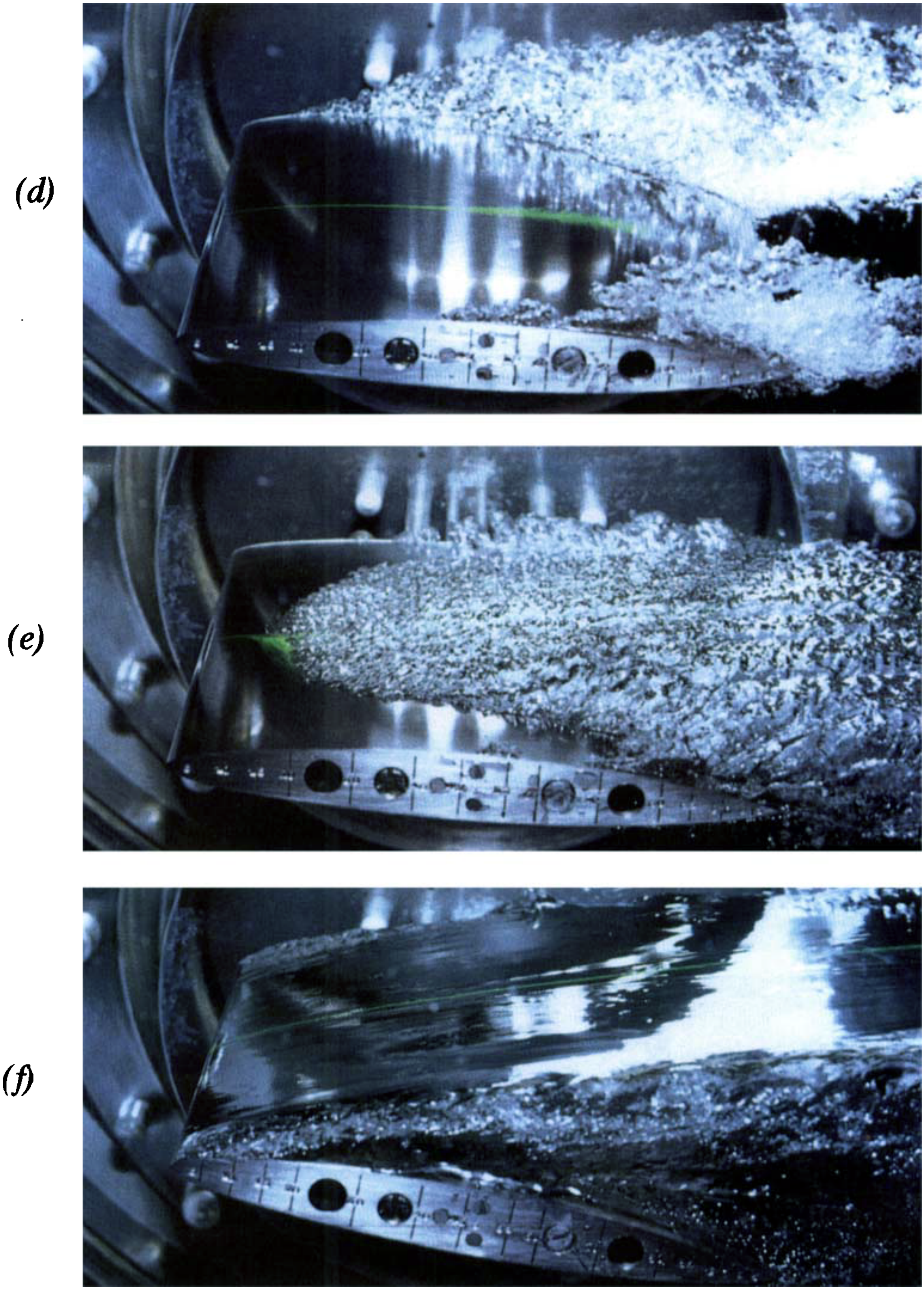

FIGURE 19. For legend see opposite.

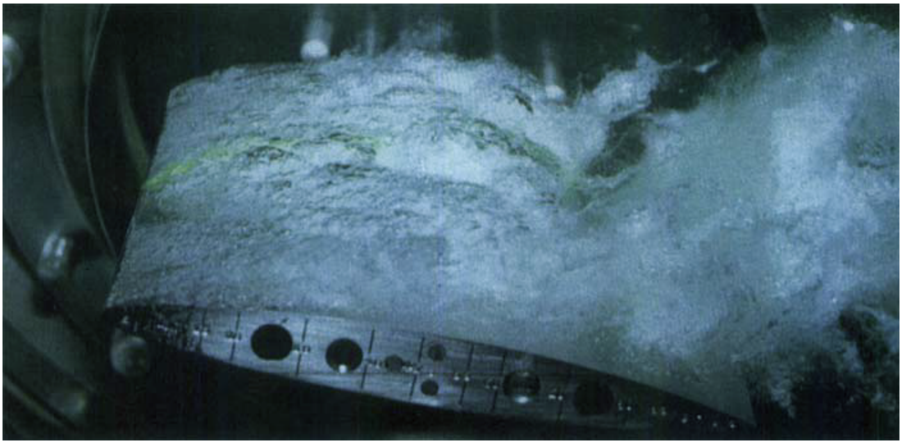

FIGURE 20. NACA 16 012; *Re* = 1 000 000; $\sigma_v = 0.81$; $\alpha = 11°$, domain 4.

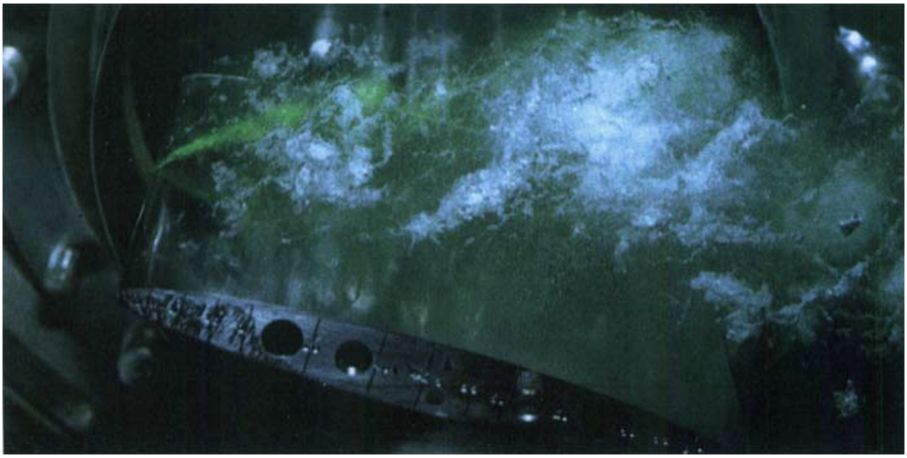

FIGURE 21. NACA 16 012; *Re* = 1 000 0000; $\sigma_v = 1.20$; $\alpha = 17°$, domain 5.

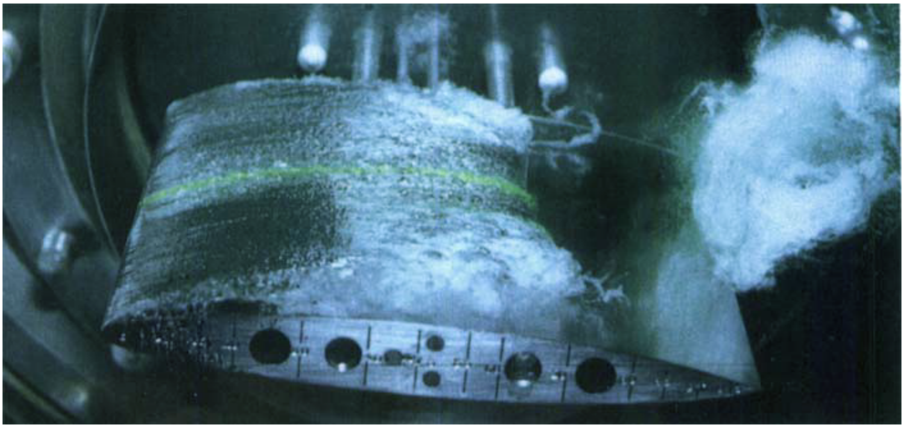

FIGURE 22. NACA 16 012: *Re* = 1 000 000; $\sigma_v = 0.81$; $\alpha = 6°$, domain 3'.

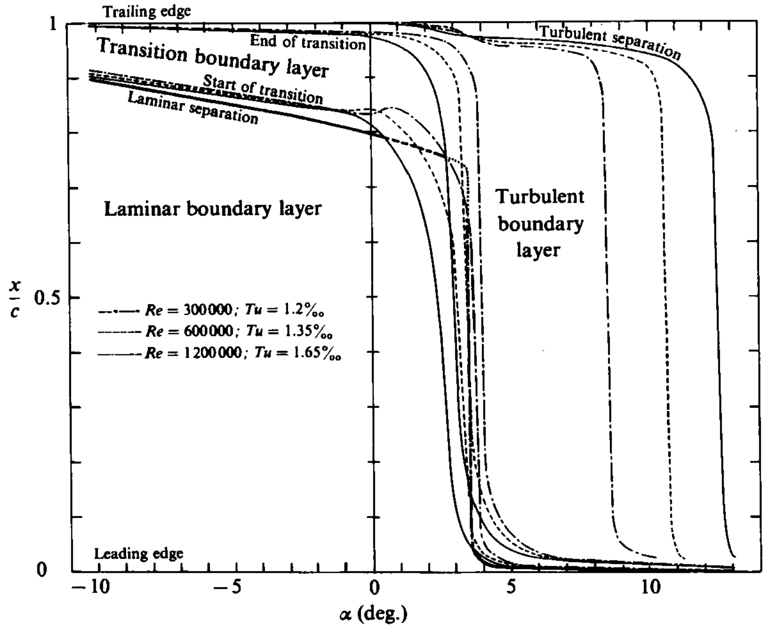

FIGURE 3. Position of boundary-layer characteristic points versus angle of attack (NACA 16012 upper side).

For instance, figure 3 shows the calculated evolution of the streamwise characteristic points of the boundary layer on the NACA 16 012 foil when its angle of attack is varied in non-cavitating flow. The experimental Reynolds number and the turbulent level are taken into account in the calculations. They influence the transition to turbulence and turbulent separation. The results compare fairly well with experiments (figure 2): in general, the steep front, which is found in the evolution curves of the slender foils such as the NACA foil or the second elliptical cylinder, coincides with the experimental jump of the boundary-layer characteristic points, to within less than $\frac{1}{2}°$. In the case of the thickest elliptical cylinder, the corresponding curves exhibit a more gradual behaviour: this fact will be compared to the behaviour of the cavity detachment.

3.2. *Pressure-coefficient calculations*

In the case of non-cavitating flows, two methods were used. The potential flow around the elliptical cylinders was first calculated by neglecting the external flow boundaries and thus by using the circle flow and the Joukowski transformation with the additional Joukowski condition being applied at the rear end of the major axis. For the NACA foil, a nonlinear method was employed which uses discrete singularities on the foil outline, and which takes into account the external boundaries: channel bottom and channel free surface. Examples of calculated pressure distribution and corresponding results on boundary layer are shown in figure 4.

At the time when the research was carried out, no method was available for the nonlinear calculation of the pressure coefficients in flows with a small cavity which closes against the body. This case, usually known as partally cavitating flow and which appears for large incidences, is not of major interest for our purposes because its cavity detachment is located in a narrow zone close to the leading edge and does

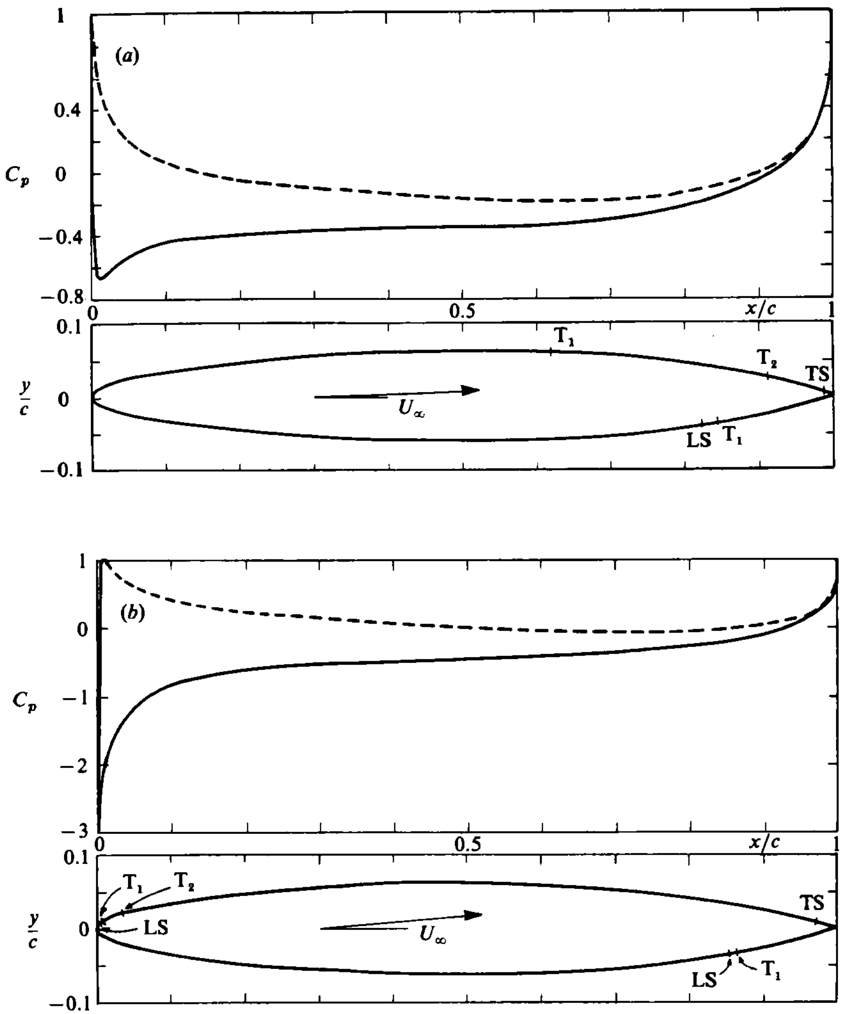

FIGURE 4. Pressure coefficient and boundary layer in non-cavitating flow (NACA 16012). $V_\infty = 12$ m/s, $Tu = 1.65$‰: —, upper side; ---- lower side; LS, laminar separation; T_1, start of transition; T_2, end of transition; TS, turbulent separation. (*a*) $\alpha = 2°$, $C_z = 0.25$; (*b*) $\alpha = 5°$, $C_z = 0.60$.

not seem to be very sensitive to modifications of the boundary layer. Thus the construction of a theoretical model for this case did not appear urgent. On the contrary, the experiment revealed that the detachment point of largely developed cavities interacts strongly with the boundary layer when the incidence values are small. There was thus a need for a computational method capable of giving a correct pressure distribution on the body and near the leading edge in order to proceed to the boundary-layer calculations, and also in the case of supercavitating flows. With this aim in mind, a linearized method matched with asymptotic expansion (Van Dyke 1970; Rowe & Michel 1975) could be chosen. Finally, it seemed better to use the numerical approach of Pellone & Rowe (1981) for treating most of the supercavitating cases of interest, i.e. with small or large values of either angle of attack or the cavity length/body chord ratio, provided cavity closure is downstream of the body.

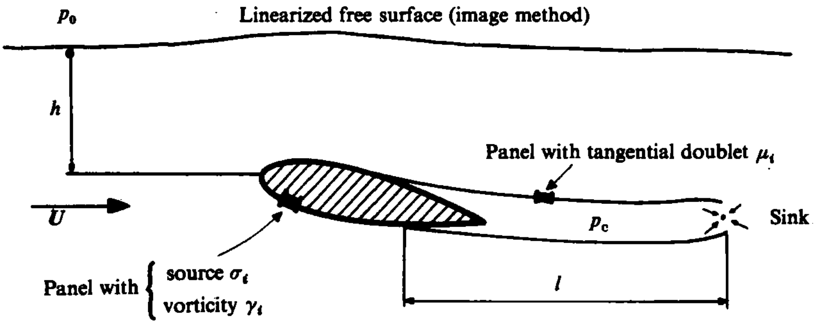

FIGURE 5. Sketch for the nonlinear model of supercavitating flow (Pellone–Rowe 1981) (the sink flow is equal to the sum of the source flows. The shape of the cavity is obtained through an iterative process).

		α		l (cm)			C_D			Boundary layer	
Re	σ_v	Exp.	Adjusted	Exp.	Adjusted	C_L	Exp.	Theor.	s_D (mm)	s_S (mm)	s_T (mm)
361000	0.075	0	1.10	14.0	9.2	0.0389	0.0172	0.0152	55	51.9	—
333000	0.083	0	0.91	11.0	7.8	0.0451	0.0173	0.0168	58	54.7	—
346000	0.107	0	1.32	7.0	5.1	0.0514	0.0236	0.0243	61	57.8	—
331000	0.114	0	1.25	4.5	4.0	0.0978	0.0230	0.0328	72	67.7	—
414000	0.106	0.97	0.98	8.0	5.4	0.0834	0.0249	0.0230	63	59.9	—
414000	0.106	2.0	2.01	8.5	5.8	0.146	0.0248	0.0233	57	—	51.1
331000	0.114	2.0	2.52	5.0	4.1	0.369	0.0305	0.0339	70	—	56.0
303000	0.137	2.0	2.98	5.5	4.5	0.293	0.0304	0.0343	59	—	48.0
414000	0.106	3.95	5.20	20.2	17.0	0.135	0.0333	0.0326	24	—	18.2
414000	0.106	4.98	6.97	30.5	32.2	0.0892	0.0427	0.0527	8.5	6.4	—

l = cavity length from leading edge.
C_L, C_D = lift coefficient, drag coefficient.
s_D, s_C, s_T = abscissa from leading edge of cavity detachment, laminar separation and transition start respectively.

TABLE 1. Slender elliptical cylinder.

In the Pellone–Rowe model, allowance is made for the channel free surface, but not for the channel bottom. The foil and the cavity boundaries are represented by a polygon made of small panels on which singularities – sources and vortices on the body, tangential doublets on the cavity – are distributed. The cavity is closed by an isolated sink. The detachment points of the cavity from the body are assumed to be known *a priori*. Thus, besides the shape of the foil, the given quantities are: its submersion depth h and angle of attack α, the cavity length l and the cavity detachment points A and B on the foil upper and lower sides (figure 5). By means of the boundary conditions and pressure continuity conditions in A and B, the model gives the pressure distribution $C_p(M) = 2(p_M - p_\infty)/\rho U^2$ and, in particular, the non-dimensional underpressure of the cavity σ. It is known (Michel 1977) that the theoretical relation $l(\sigma)$ which is obtained from such a model, often needs to be adjusted on the basis of experimental results. Thus, in some circumstances, especially when it appeared necessary to obtain good correlation between model and experiments concerning the parameter σ and the lift coefficient C_L, the values of l and α introduced

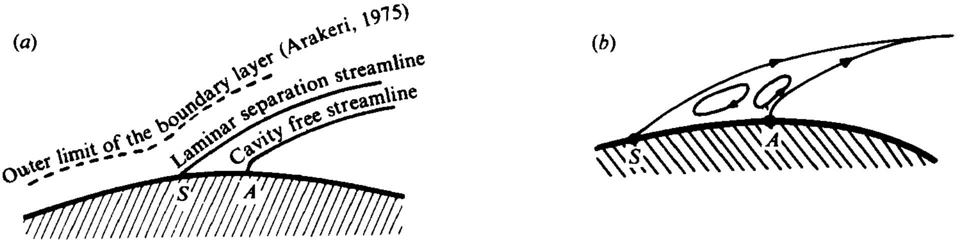

FIGURE 6. The neighbourhood of A and S (paradox).

in the model were modified so as to obtain the experimental values of σ and C_L. Examples of such adjusted values will be found in table 1. In most cases, it seemed better to emphasize flow geometry and these corrections were not made.

At this point, it is worth pointing out two difficulties which affect flow representation in the detachment vicinity. The first difficulty appears when the cavity detachment point A and the laminar separation point S are juxtaposed (figure 6*a*): the cavity free streamline and the laminar separation streamline come from two neighbouring stagnation points, in other words they determine a downstream sink flow without any upstream source. This difficulty does not exist if laminar separation is defined by the sudden thickening of the boundary layer, or if allowance is made for recirculation zones between S and A (figure 6*b*). Another way consists of taking into account either the mass transfer between the vapour and liquid phase or possibly the locally three-dimensional unsteady behaviour of the flow. The photographs given here illustrate the local character of the paradox and suggest that the ways of getting round it are reasonable.

The second difficulty appears when the scheme of non-viscous fluid in irrotational flow is used for calculation of the pressure distribution (Wu 1972). The two-dimensional solution $\omega(z)$ (where ω stands for $\log(q/q_c) - i\theta$; q is the flow speed, q_c the q value on the cavity boundary, θ the streamline slope) behaves as $ik(z-z_A)^{\frac{1}{2}}$ in the vicinity of the detachment point A if A is anywhere on the wall. This behaviour leads to two unrealistic consequences: (1) the cavity boundary has an infinite curvature at A (Villat 1914), so that there is a risk of it intersecting the wall downstream of A; and (2) the longitudinal pressure gradient also becomes locally infinite: near A, $\partial p/\partial s \simeq k\rho q_c^2/2|z_A - z|^{\frac{1}{2}}$ (Armstrong 1953). If an attempt is made to avoid this behaviour through the hydrodynamic scheme, the A position has to be determined so as to cancel the quantity k. The free-streamline curvature and the wall curvature are then equal at A and the pressure gradient, which becomes continuous, takes the zero value it possesses on the cavity. This 'smooth detachment condition' had been proposed by Villat within the framework of the old wake theory, and later by Armstrong. It was subsequently considered by Pellone & Rowe who gave it a workable form. However, after examination, it appears that in most situations the experimental detachment is not predicted well by the smooth-detachment criterion.

Thus, in the present work, a boundary-layer flow is superimposed on a potential flow in which the pressure-gradient singularity is not removed. This is not detrimental to the results of the boundary-layer calculations because it is possible to stop the step-by-step process in the computation before reaching the influence zone of the singularity (figure 7): any artificial laminar separation which would be due to the abrupt adverse pressure gradient between A' and A is avoided. Of course, a considerable amount of work would be necessary in order to improve the model of

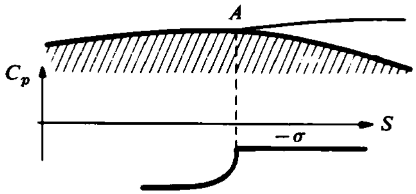

FIGURE 7. Pressure coefficient in the neighbourhood of detachment A.

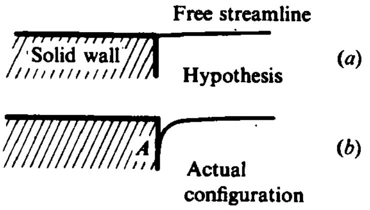

FIGURE 8. Shearaway.

the detachment region. In the case where the detachment is imposed by a discontinuity of the solid-wall slope – termed shearaway by Ackerberg (1970, 1975) – viscosity and interfacial properties of the liquid (with its vapour and the solid material) play a major role since experience often shows configurations such as that sketched in figure 8(*b*), the topology of which differs considerably from that which was first envisaged (figure 8*a*). The same mechanisms are also present in the case of a wall with continuous curvature: this appears clearly in the contact angle of the free streamline at detachment, which is not zero, as assumed by potential-flow theory, but depends on the flow velocity, for example in the case of the circular cylinder. To summarize, it is believed that the approach which is proposed here is convenient for describing the overall characteristics of largely cavitating flows around slender bodies, but it must be complemented by a careful examination of the local influences close to the cavity detachment.

4. Preliminary results

In this section, the preliminary results obtained with the circular cylinder and the two elliptical cylinders are presented.

4.1. *Circular cylinder*

In the case of the circular cylinder, results are restricted to measurements of two global, geometrical characteristics of cavity detachment (figure 9):

(*a*) its position given by the angle ϕ between stagnation and detachment points;

(*b*) its direction given by the angle ψ between the tangents to the cylinder and to the cavity at detachment.

These two variables are expressed in terms of the Reynolds number and the cavitation parameter. As the cylinder has a diameter of 1 cm, the Reynolds number varies between 25000 and 130000 (figure 1) and the boundary layer exhibits laminar separation under non-cavitating conditions.

Measurements are made from photographs. The upper and lower bounds of the cavity are digitized over a length of 0.75D to D with 100 points each. They are

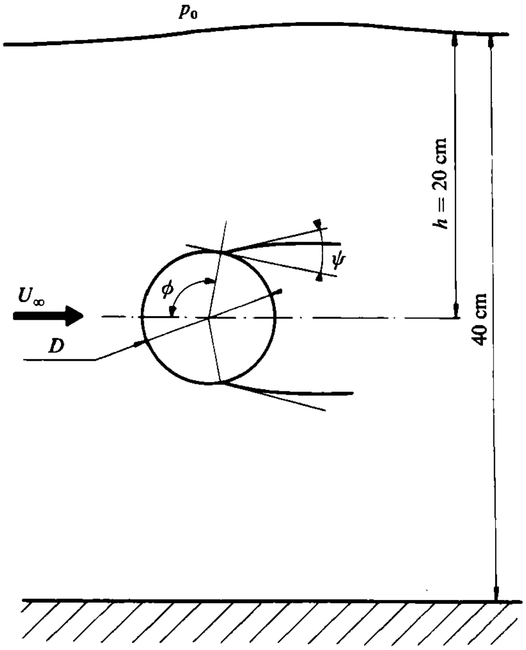

FIGURE 9. Sketch of cavity detachment from cylinder.

smoothed with a fourth-order polynomial and the two angles ϕ and ψ are determined from calculation of the intersection of these polynomials with the section of the cylinder. No significant difference between the two detachments is found.

For each angle, mean and r.m.s. values are calculated on a sample of twenty-eight values. In our range of variation of Reynolds number and cavitation number, mean values of ϕ and ψ are fairly well represented by the two formulae:

$$\left.\begin{aligned}\phi &= 72.2+7.494\sigma+\frac{915000}{Re}+\frac{180000\sigma}{Re};\\ \psi &= 1.68+10.93\sigma+\frac{1860000}{Re}-\frac{198300\sigma}{Re}.\end{aligned}\right\} \quad (1)$$

The estimation of uncertainties on mean values from r.m.s. values gives on average ±1.4° for ϕ and ±3.7° for ψ.

For high values of the cavitation parameter, the detachment is defined with less accuracy as shown in figure 10, where it can be seen that the cavity tends to be no longer attached to the cylinder. This is characteristic of the subcritical regime (in this case $Re \lesssim 270000$) in which cavitation inception occurs within the wake and not attached to the body. On the other hand, experiments carried out on a bigger cylinder ($D = 5$ cm) have shown that, in the supercritical regime, cavitation appears first within the laminar separation bubble in the form of band-type cavitation.

Figure 11 shows the strong influence of Reynolds number on detachment at $\sigma_v = 0.62$. It can clearly be seen that, when the Reynolds number is increased, the detachment moves upstream and becomes more and more tangential to the cylinder. The same trends are shown on figures 12 and 13 when the cavitation number is decreased. An important point is that the influence of the streamwise velocity is still

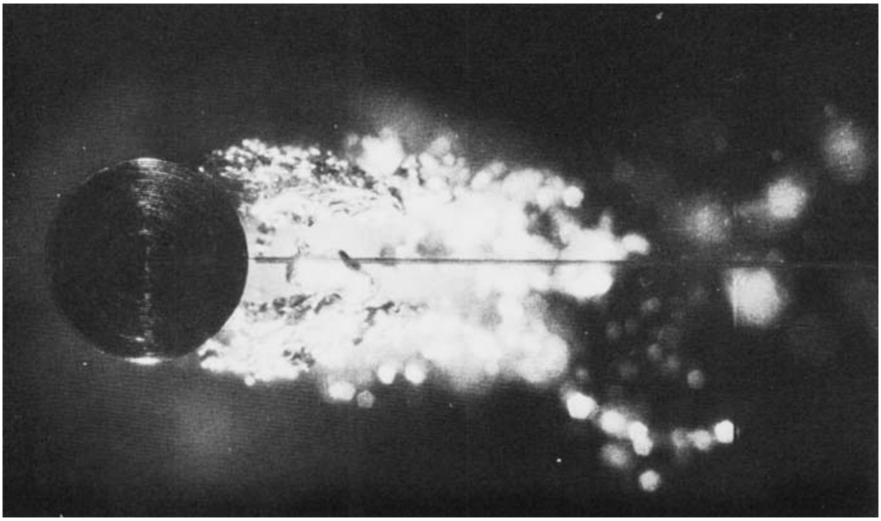

FIGURE 10. Circular cylinder: $Re = 25000$, $\sigma_v = 1.0$.

present for lower values of the cavitation number, i.e. for the case of supercavitating flows.

Concerning the position of detachment ϕ, our experimental results are compared in figure 12 with the prediction given by Arakeri's (1975) correlation obtained from experiments on axisymmetric bodies. General trends appear to be well reproduced by Arakeri's correlation, but the difference between numerical values may exceed 20°.

Another comparison is made with experimental results reported by Oba *et al.* (1980) and obtained with a brass cylinder of 15 mm diameter and a Reynolds number of 190000. Though our maximum Reynolds number is 105000, a comparison is possible by extrapolating our data by means of (1). Figure 12 shows good agreement for detachment position ϕ whereas figure 13 illustrates considerable differences for ψ particularly in the variation with σ_v: our experiments indicate that detachment becomes more and more tangential as σ_v decreases, i.e. as cavitation develops.

4.2. *Elliptical cylinders*

In the case of elliptical cylinders, the boundary layer does not necessarily continue to be laminar under non-cavitating conditions, but may exhibit a transition to turbulence when the angle of attack is increased. Thus, much more information can be expected on the interaction between developed cavitation and boundary layer.

Results of calculations of the boundary layer on the upper side of the thicker elliptical cylinder under non-cavitating conditions are plotted on figure 14(*a*), in addition to measurements of the upper detachment position. For low angles of attack ($\alpha \lesssim 1°$), the subcavitating boundary layer is laminar and separates at $x/c \simeq 0.9$; for $\sigma_v = 0.4$, the cavity which is only slightly developed, detaches from the body close to the subcavitating laminar separation point. This is in good agreement with other results on cavitation inception (Alexander 1968; Arakeri & Acosta 1973; Van der Meulen 1980). When the cavitation number decreases, the detachment moves upstream. For higher angles of attack ($\alpha \gtrsim 1°$), the subcavitating boundary layer becomes turbulent and the point of transition, as well as the cavity detachment point (figure 14*a*, *b*), moves gradually upstream with increasing angle of attack.

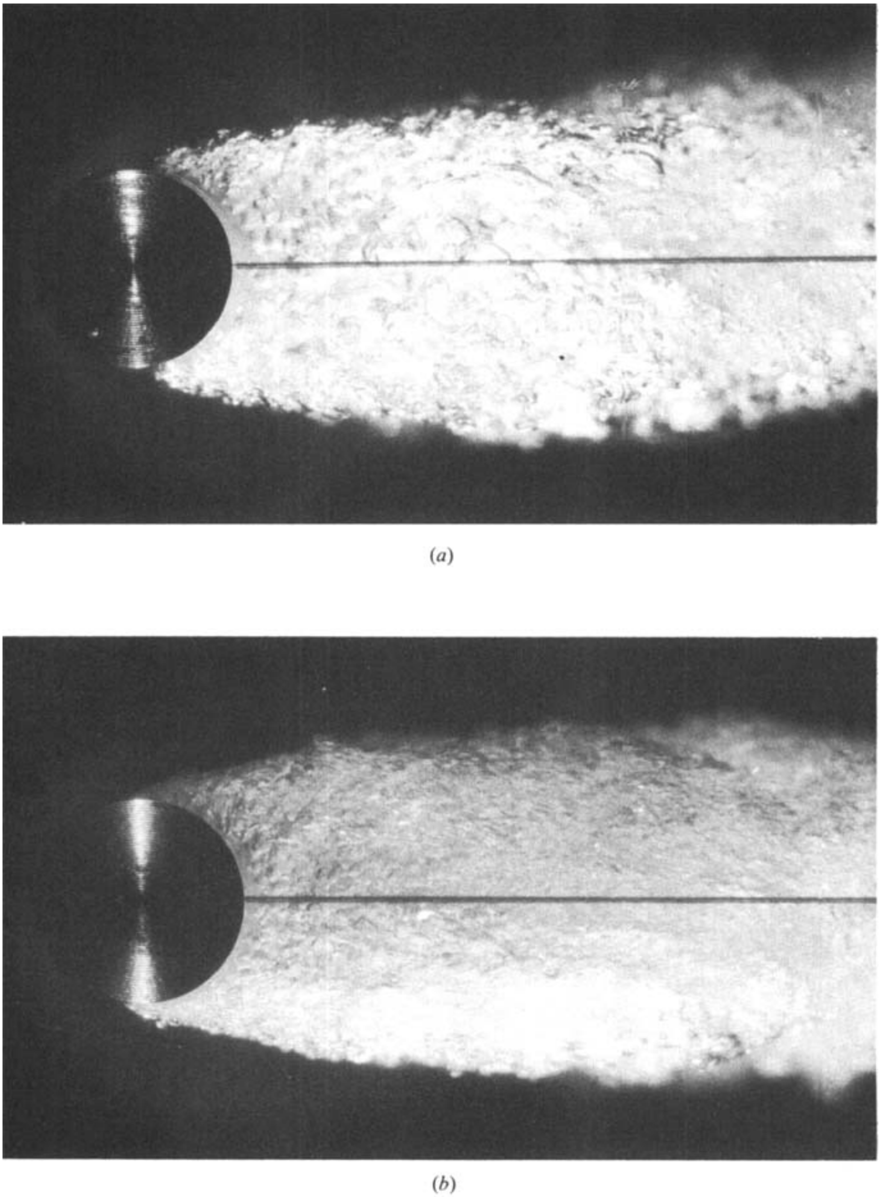

FIGURE 11. Circular cylinder: $\sigma_V = 0.62$. (a) $Re = 55000$; (b) $Re = 104000$.

This is not the case for the slender elliptical cylinder for which the start of transition jumps from $x/c \simeq 0.9$ at $\alpha = 1°$ to $x/c \simeq 0.2$ at $\alpha = 3°$, for $Re = 960000$ (here, and in that which follows, Re is based on the chord $2a$ or c), as shown on figure 15(a). Under cavitating conditions (figure 15b), a similar jump is observed for the detachment between 2° and 4°. For high values of the cavitation parameter ($\sigma_V > 0.11$), cavitation disappears in this narrow domain of incidence; for low values of the cavitation number, a cavity still exists, but the detachment is very irregular all along the span.

When the Reynolds number increases, with all other conditions the same, the

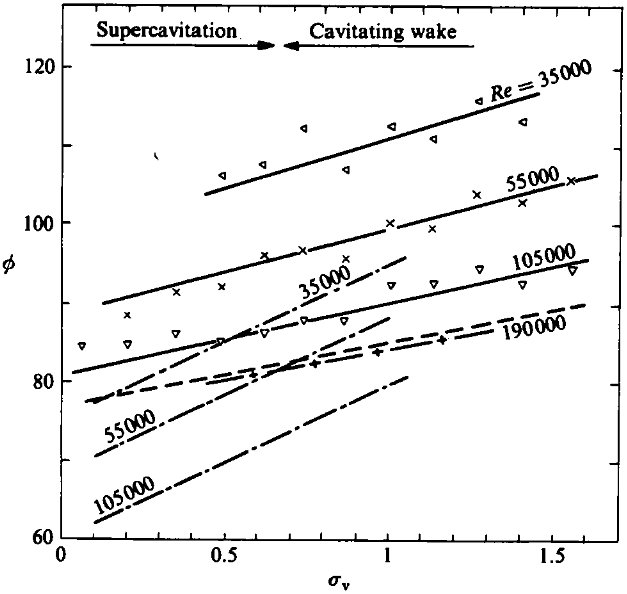

FIGURE 12. Circular cylinder; position of cavity detachment versus cavitation parameter: ——, our experimental results; —·—, Arakeri; ----, extrapolation of our results for $Re = 190000$; — + —, Oba.

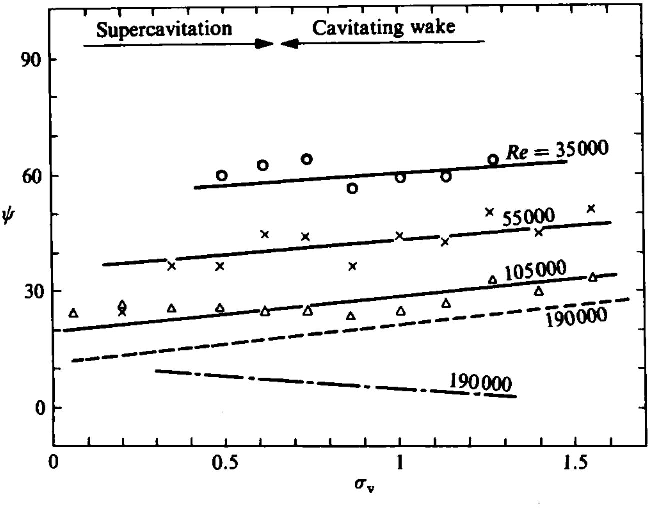

FIGURE 13. Circular cylinder; direction of cavity detachment versus cavitation parameter: ——, our experimental results; ---, extrapolation of our results for $Re = 190000$; —·—, Oba.

detachment moves upstream (figures 14*b* and 15*b*). However, this shift is much smaller for the thick elliptical cylinder than for the circular one, and it is hardly perceptible for the slender elliptical cylinder. For slender bodies, the influence of the streamwise velocity on detachment appears to be of minor importance.

Visualization of the boundary layer under cavitating conditions by injection of coloured water at the leading edge shows that the boundary layer is always laminar up to detachment and exhibits a laminar separation a few mm upstream of the

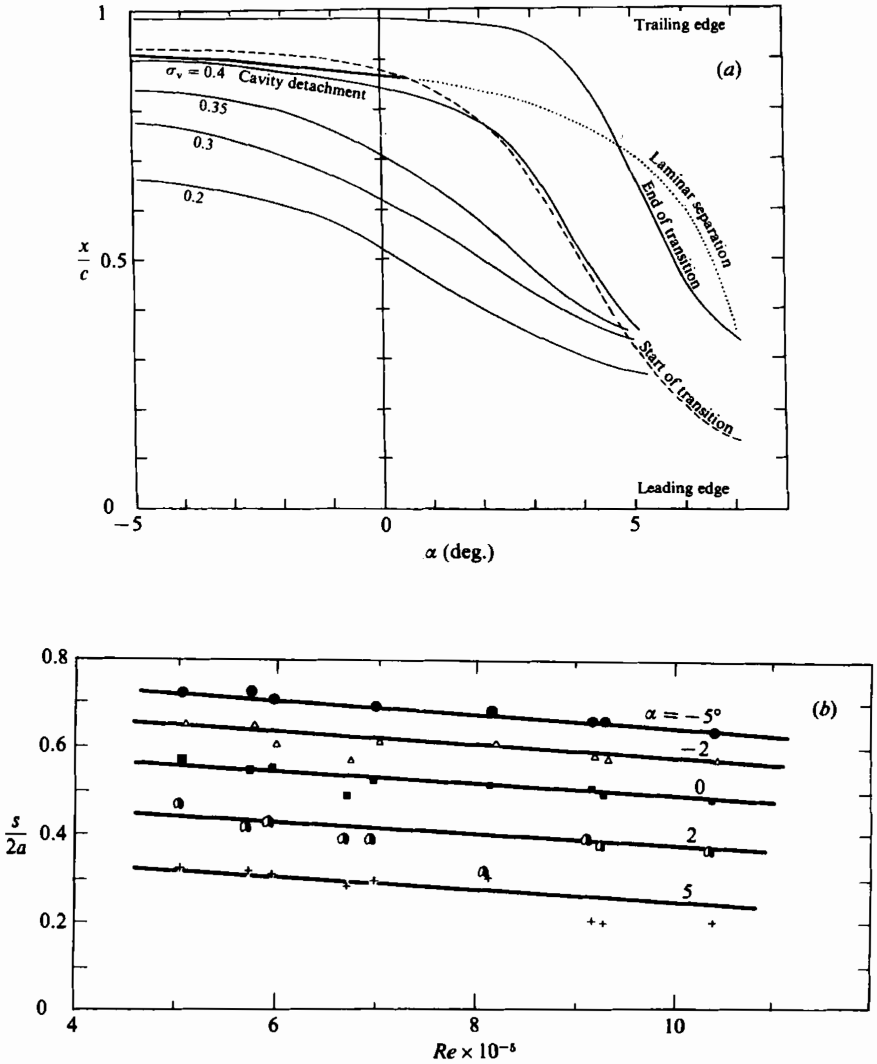

FIGURE 14. Thick elliptic cylinder: position of characteristic points. (*a*) Start and end of transition for $Re = 960000$, $Tu = 1.65$ ‰ (calculated), laminar separation (calculated); cavity detachment for $\sigma_v = 0.4-0.3$ and 0.2 and $Re = 800000$ (measured); (*b*) cavity detachment for $\sigma_v = 0.2$ (measured).

detachment for low and high angles of attack ($\alpha \lesssim 2°$ and $\alpha \gtrsim 4°$). This is corroborated by the results of calculations presented in table 1. For these calculations, the experimental upper and lower detachment positions are used as data for the potential cavitating flow computation; the cavity length and angle of attack are fitted so that the calculated cavitation number and lift coefficient equal the corresponding experimental values. For $\alpha_{\text{exp}} = 0°$, 1° and 5°, the boundary-layer calculation on the wetted part of the foil predicts a laminar separation a few mm upstream of the detachment, as observed experimentally. For intermediate values of α_{exp} ($\alpha_{\text{exp}} = 2°$ and 4°), the calculation predicts the start of transition upstream of the detachment, which tends to be in contradiction with the experiment. In §6, where this domain of incidence is studied in more detail, it will be shown that the boundary-layer

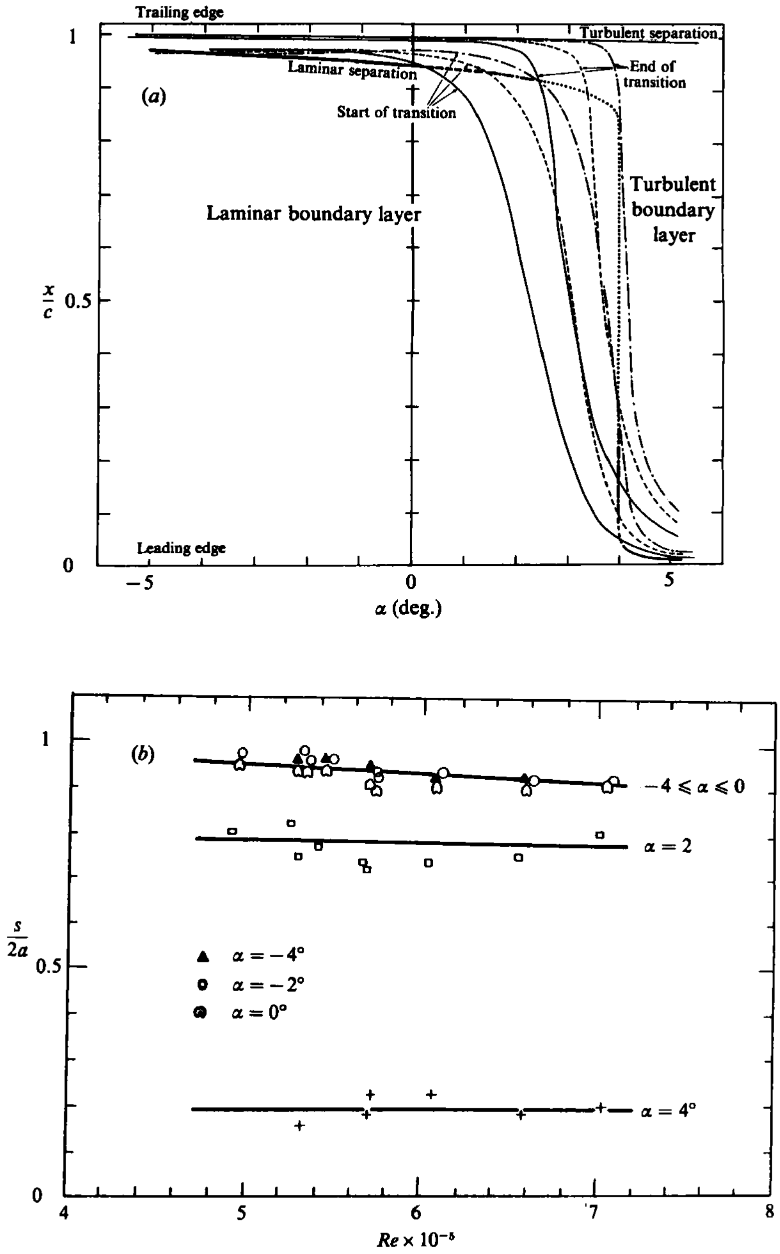

FIGURE 15. Slender elliptic cylinder: position of characteristic points. (*a*) start and end of transition (calculated): — - —, $Re = 240000, Tu = 1.2$ ‰; ----, $Re = 480000, Tu = 1.35$ ‰; ——, $Re = 960000$ $Tu = 1.65$ ‰; laminar and turbulent separation (calculated). (*b*) Cavity detachment for $\sigma_v = 0.13$ (measured).

behaviour is very sensitive to the detachment position, which is experimentally badly defined in this range of incidence.

In addition, measurements of lift and drag coefficients are carried out on the slender elliptical cylinder. The variation of lift coefficient is approximately linear for low angles of attack ($-3° \lesssim \alpha \lesssim +3°$) for which cavity upper detachment occurs at the

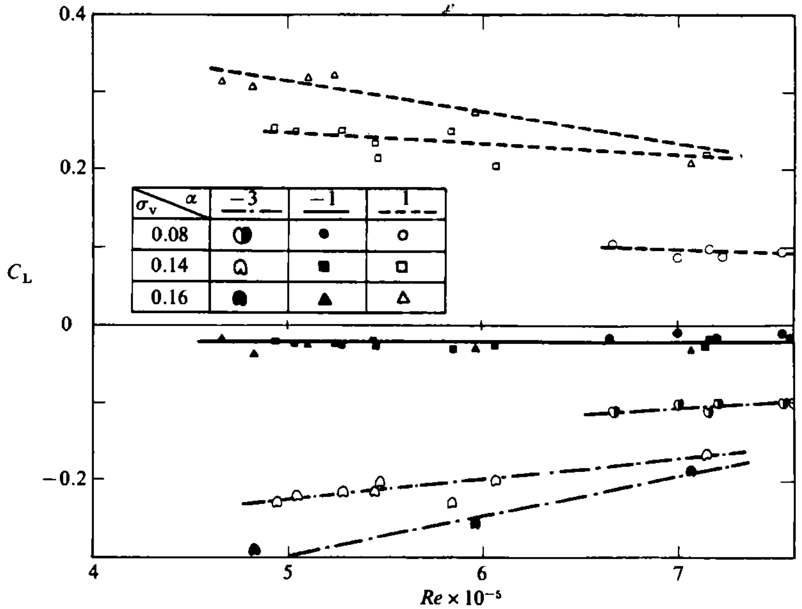

FIGURE 16. Slender elliptic cylinder; measured lift coefficient: ----, $\alpha = 1°$; ——, $\alpha = -1°$; —·—, $\alpha = -3°$.

rear of the foil. For higher angles of attack, when the detachment jumps ahead, the lift coefficient drops. Figure 16 shows that the influence of Reynolds number on the lift coefficient as well as the influence of cavitation number disappear at $\alpha \simeq -1°$, which corresponds approximately to zero lift and for which upper and lower detachments are symmetrical. Except for this particular value of incidence, the greater the cavitation number, the more sensitive the decrease in lift becomes, when increasing the Reynolds number.

The few preliminary results discussed in the present section definitely show that a strong interaction exists between developed, attached cavitation and boundary layer. By interaction, two coupled aspects are implied as follows.

(*a*) The influence of cavitation development on the characteristics (such as laminar separation or transition) of the boundary layer on the wetted part of the cavitating body.

(*b*) The influence of the boundary-layer state (laminar or turbulent) and behaviour (separation or transition) on cavitation patterns and cavity detachment.

Two facts appear to be particularly significant with respect to this interaction: first, the cavity detachment from the downstream part of the foils in the case of small angles of attack – which was not observed previously, to our knowledge, in the case of large cavities; secondly, the elimination of developed cavitation by natural transition to turbulence in the case of the slender elliptical cylinder. Concerning the second point, Arakeri & Acosta (1973) reported that only artificial excitation of transition on the nose of axisymmetric bodies could delay the appearance of cavitation.

5. NACA 16 012 – experimental results

In this section, a comprehensive description is given of the boundary layer and the different cavitation patterns which develop on the upper side of a NACA 16012 foil, according to the values of cavitation number, angle of attack and Reynolds number.

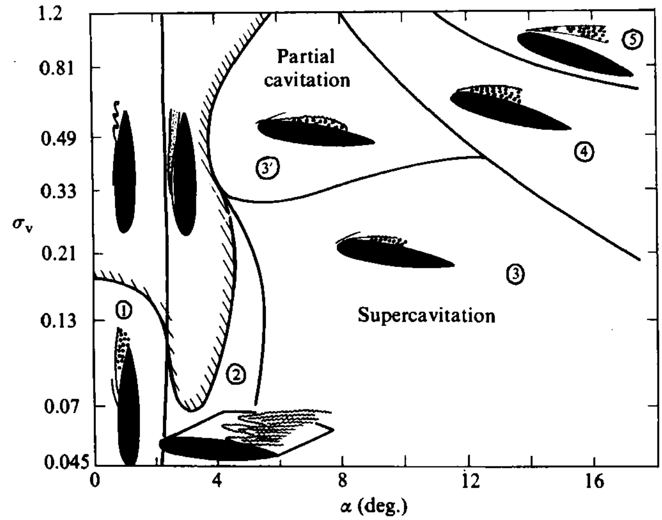

FIGURE 17. NACA 16012: observed cavitation patterns at $Re = 1000000$.

As mentioned previously, the influence of Reynolds number is not very significant for slender bodies such as the NACA 16012 foil. Thus, the two parameters which play a major role are cavitation number and angle of attack. As before, the global behaviour of the boundary layer is deduced from visualization by dye injection.

Concerning the fully wetted flow, results of boundary-layer visualization have already been presented in §2. Boundary-layer behaviour is summarized in figure 3, deduced from calculation, and is in good agreement with experimental results. It is qualitatively similar to the case of the slender elliptical cylinder. At $Re = 600000$, for instance, the upper boundary layer is laminar and exhibits a laminar separation at $x/c \simeq 0.8$–0.9 up to a 2° angle of attack. Between 2° and 3.5°, transition to turbulence occurs and jumps from $x/c \simeq 0.8$ to $x/c \simeq 0.1$. At 3.5°, a laminar separation bubble appears near the leading edge; the boundary layer is turbulent on most of the upper side. At 11°, stall occurs.

Concerning the cavitating flow, different domains of the (α, σ_v)-plane are considered, corresponding to different cavitation patterns and boundary-layer behaviour as they can be deduced from observations. They are shown on figure 17 at $Re = 10^6$ and each is illustrated by a photograph (figure 18, plates 2 and 3, and figures 20–22, plate 6). Another series of photographs is given at $Re = 600000$ (figure 19, plates 4 and 5).

The surface of the cavity may appear glossy or wavy, and there often exists on the cavity a point of transition from a glossy to a wavy aspect. It may be that this particular cavity surface point corresponds to a point of transition to turbulence in the liquid flow close to the cavity detachment. This interpretation is corroborated by the fact that, for moderate values of the cavitation number, at which the cavity disappears for intermediate angles of attack, there is approximately continuity between the glossy–wavy transition point on the cavity under cavitating conditions and the turbulence transition point on the foil under non-cavitating conditions, as shown on figure 23.

At low angles of attack (domain 1 – figures 18*a* and 19*a*), detachment takes place at the rear of the foil. The flow on the wetted part of the foil is laminar and separates

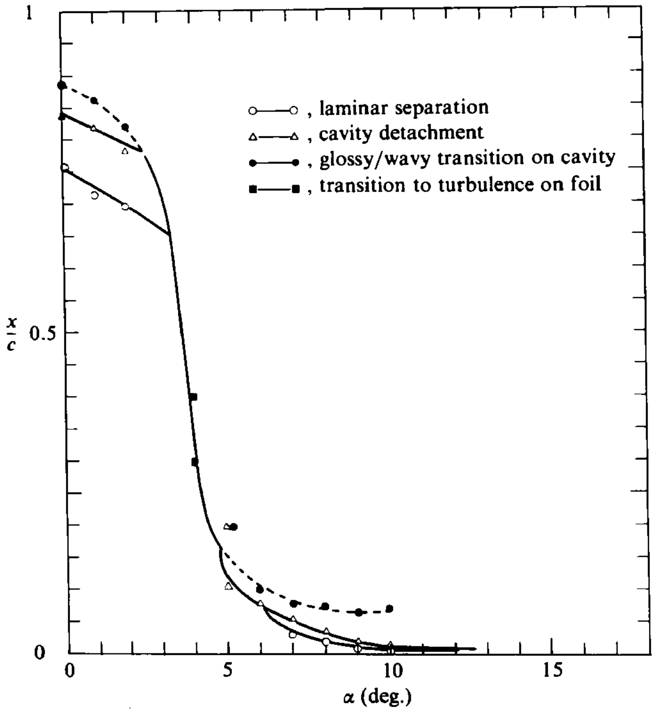

FIGURE 23. NACA 16012: measured position of characteristic points for $Re = 600000$ and $\sigma_v = 0.17$.

a little before detachment. The glossy appearance of the cavity near detachment indicates that the separated boundary layer is still laminar at the very beginning of the cavity. Transition to turbulence is assumed to occur a little further along the cavity boundary, at the point where it becomes wavy.

When the angle of attack increases, the glossy–wavy transition on the cavity comes nearer to detachment. When it reaches detachment, the cavity is swept away for moderate values of the cavitation parameter, and transition takes place on the foil (figure 19*d*); there may be some separated bubbles which explode on the upper side. For sufficiently low values of the cavitation parameter ($\sigma_v \lesssim 0.07$ domain 2 – figure 18*b*,*c*) a cavity still exists; the detachment is very three-dimensional and the boundary layer is laminar up to detachment. Although the cavity often exhibits a little glossy part near detachment, which remains very limited crosswise and which is generally ahead of the rest of the cavity, it usually appears wavy from detachment. Contrary to the other cases, the cavity is not very stationary near detachment: the coloured thread is deflected by the cavity at the mercy of its movement. The cavity may even disappear during a small lapse of time; then the boundary layer is turbulent and bubbles explode on the upper side. As a glossy part is observed it can be surmised that, in this narrow domain of incidence, detachment is still controlled by laminar separation. However, contrary to the other cases, such a configuration is likely to be unstable since it seems very sensitive to small disturbances and does not exist two-dimensionally along the entire span; on parts of the foil span, laminar separation is probably replaced by transition to turbulence which makes cavitation vanish on the corresponding part of the span.

When the angle of attack continues to increase, detachment becomes very

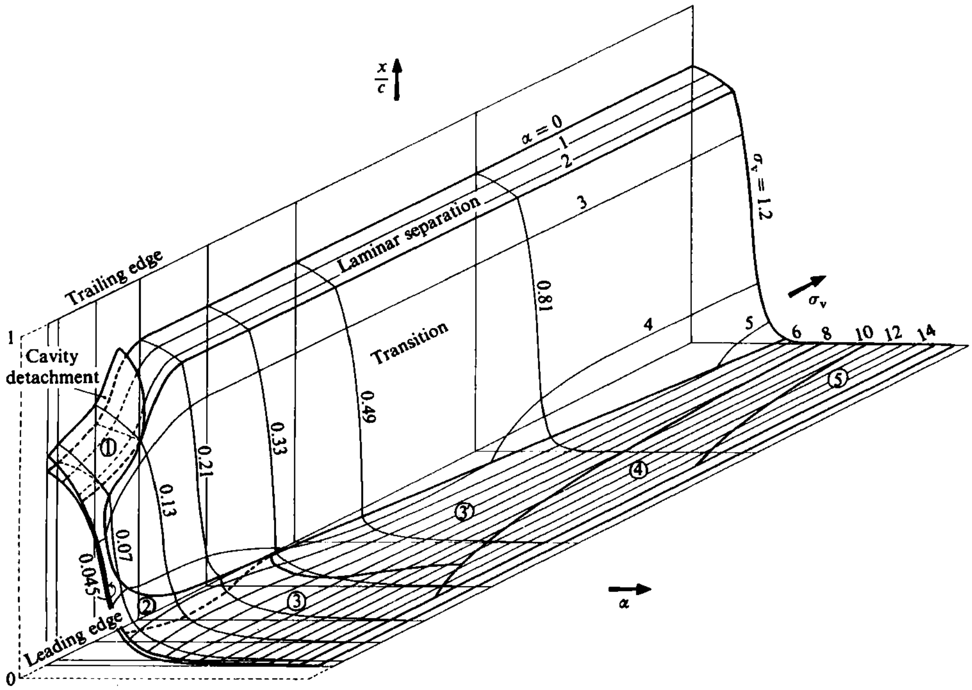

FIGURE 24. NACA 16012: measured position of characteristic points for $Re = 1000000$.

two-dimensional again. It is located near the leading edge. Upstream of cavity detachment, the dye is inclined to stagnate and to spread crosswise. This indicates a recirculating zone which characterizes laminar separation. For low cavitation numbers, a supercavitation situation occurs (domain 3 – figures 18*d*, *e*, *f*, 19*f*) whereas cavitation is partial for high cavitation numbers (domain 3′ – figure 22).

When the angle of attack and the cavitation number increase, the cavity is no longer filled only with vapour, but is made up of a two-phase mixture (domain 4 – figure 20). Then, cavitation is no longer attached to the foil; it appears in the free-shear layer as two-dimensional cavitating structures which are often shed periodically (domain 5 – figure 21).

If a third dimension is added to figure 17, made of the reduced abscissa x/c, then it is possible to represent the position of the different characteristic points (detachment, separation, transition). From the above interpretations and measurements on photographs, a diagram is deduced as shown in figure 24. In particular, it appears that, if the foil is held at a 4° angle of attack, when the cavitation number decreases from 1.2 to 0.045: partial cavitation appears first; then, it disappears and the flow becomes non-cavitating; finally, supercavitation occurs.

This fact, which is perfectly repeatable and reversible, is very surprising. It shows that a decrease in pressure may lead to the disappearance of a certain type of cavitation (in this case partial cavitation) without it being replaced by any other type of cavitation. Thus, it can be inferred that in such circumstances cavitation is not compatible with the state of the boundary layer.

It can also be noted that, with decreasing cavitation number, the detachment moves upstream under supercavitating conditions whereas it moves downstream under partial cavitating conditions (figure 25).

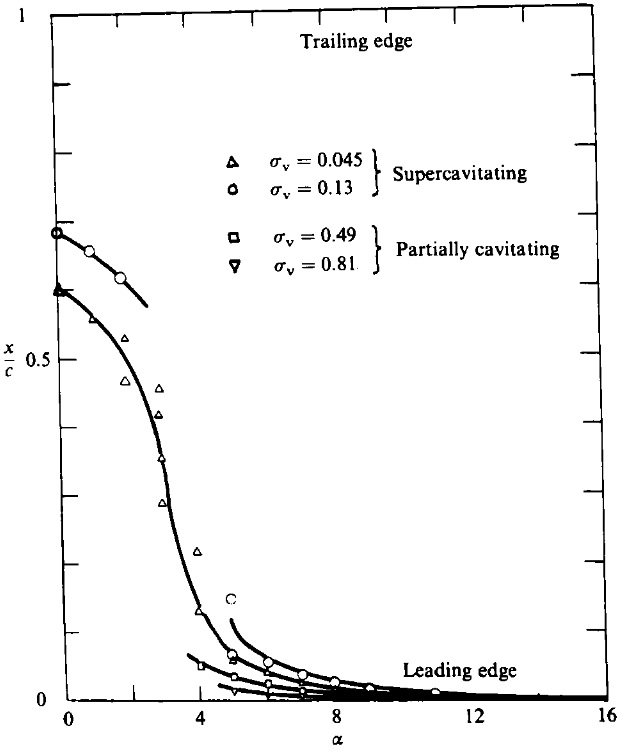

FIGURE 25. NACA 16012: measured position of cavity detachment for $Re = 1000000$.

This section confirms that cavity detachment takes place just downstream of the boundary-layer separation, but not at the minimum pressure point. It is precisely the corresponding adverse pressure gradient which makes the boundary layer separate. From computation results given in the next section, the pressure is lower than vapour pressure on most of the wetted part except near the leading edge; it may even become negative. In practice, this is possible if the minimum pressure is not low enough to make nuclei explode, which is the case in our experiments for which the minimum pressure is estimated to be -15000 Pa, whereas the nuclei critical pressure is about -20000 Pa.

6. A detachment criterion

Experiments presented in the preceding section show that a cavity detachment takes place behind a laminar separation. Thus, it is consistent to test the following cavity detachment criterion: among all the theoretically possible detachment points, the actual detachment point is the one for which the computation predicts a laminar separation just upstream. As a corollary, it can be assumed that, if no laminar separation is predicted in front of a theoretical cavity, no attached cavity can actually exist.

It follows that computations have to be carried out in two steps.

(*a*) The pressure coefficient distribution on the wetted part of the foil is determined by a nonlinear calculation of the cavitating potential flow. At the present time this calculation, presented in §3.2, is restricted to supercavitation. Among the various

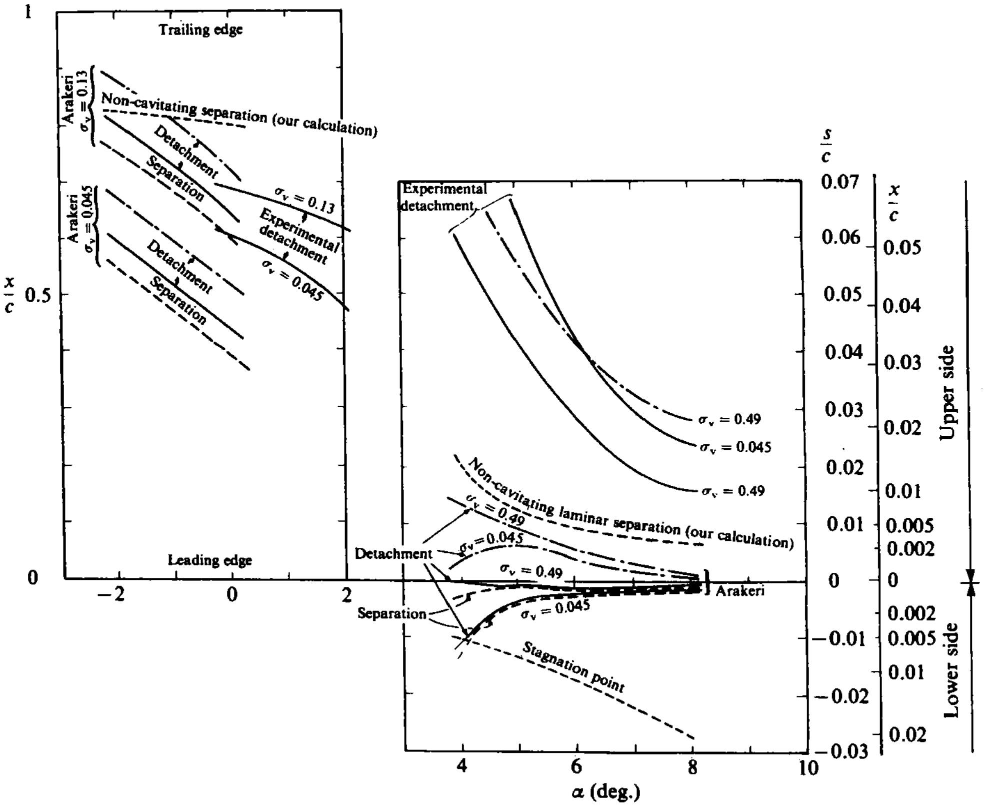

FIGURE 26. Application of Arakeri's correlation to the case of the NACA 16012: —·—, $Re = 300000$; ——, $Re = 1000000$.

geometrical data (angle of attack, cavity length, etc.), greatest interest lies in the cavity detachment position. The cavity length is adjusted so that the cavity pressure equals the vapour pressure.

(*b*) The boundary layer is calculated on the wetted part of the foil by the integral method presented in §3.1. The main calculated parameters are, in addition to the different boundary-layer thicknesses, the positions of the characteristic points of the boundary layer and, especially, the laminar separation, if any.

The application of the criterion consists of moving the detachment point on the foil; for each of its successive positions, the position of laminar separation, if any, is determined and is compared to the position of detachment. By means of the above-mentioned criterion, it is possible to determine the actual cavity detachment position which is compared with the measured one.

The previous criterion lacks a little precision. In order to obtain a more accurate prediction, the distance between laminar separation and cavity detachment should be specified. This was achieved by Arakeri (1975), as mentioned in the introduction. The complete Arakeri's correlation has already been tested on a circular cylinder (see §4.1). It is discussed below for the case of the NACA 16012 foil (figure 26). At around 3°, the correlation cannot be applied since the non-cavitating boundary layer does not exhibit a laminar separation but a transition to turbulence. At 1° and 2°, it cannot be applied either, since it leads to a negative abscissa of laminar separation under

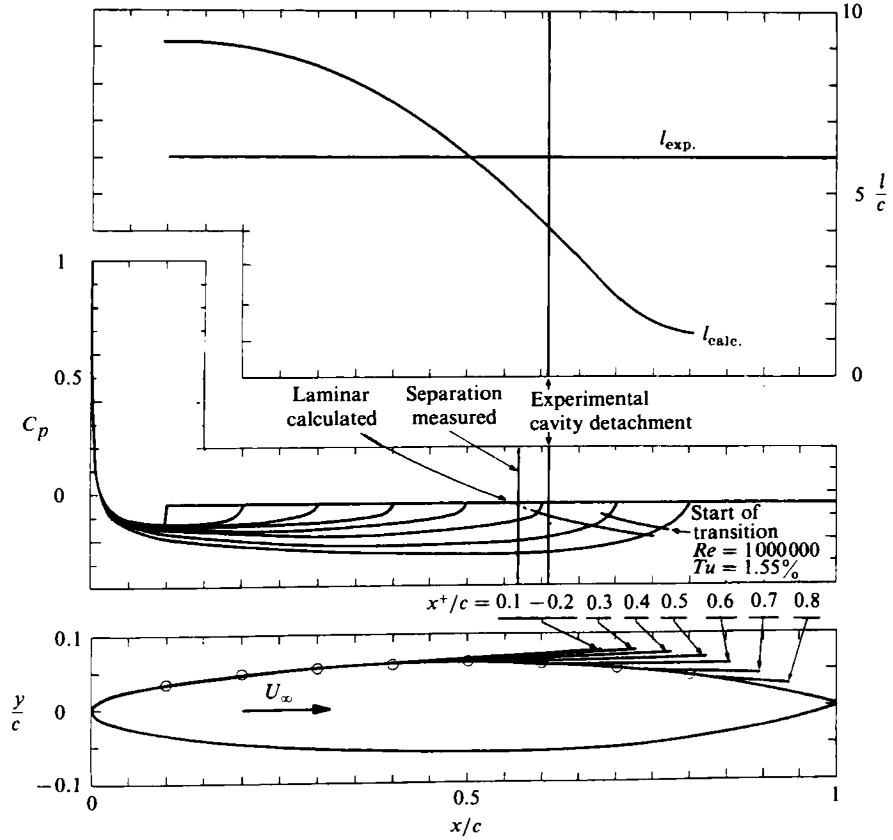

FIGURE 27. NACA 16012: numerical results of supercavitating potential flow and boundary-layer computations for $\alpha = 0$ and $\sigma_v = 0.045$. *Note:* for $x^+/c = x^-/c = 0.1$, the cavity cuts the foil.

supercavitating conditions. As a matter of fact, two adverse-pressure-gradient zones exist. The first corresponds to the trailing edge, and the second to the negative-pressure peak which appears near the leading edge at high angles of attack (see figure 4). A low-pressure-gradient zone exists between these two zones. Under non-cavitating conditions, for angles of attack of 1° and 2°, the laminar separation point belongs to the first adverse-pressure-gradient zone, whereas the minimum pressure point belongs to the second zone. There appears to be very little correlation between these two points and they are a wide distance apart. This explains why the forward shift of laminar separation, which is directly proportional to this distance, is unrealistic, according to the correlation. For low and high angles of attack ($\alpha < 0°$ and $\alpha > 4°$), Arakeri's correlation gives a realistic prediction which may, however, significantly differ from experiments. Below, Arakeri's correlation is not used, even for the prediction of the distance between laminar separation and detachment under cavitating conditions.

To return to the proposed criterion, calculations show that there is a given position for which, with a detachment point before it, no separation occurs and, with a detachment point behind it, separation occurs. It is the immediate vicinity of this particular position which is considered for prediction and compared with the experimental detachment point.

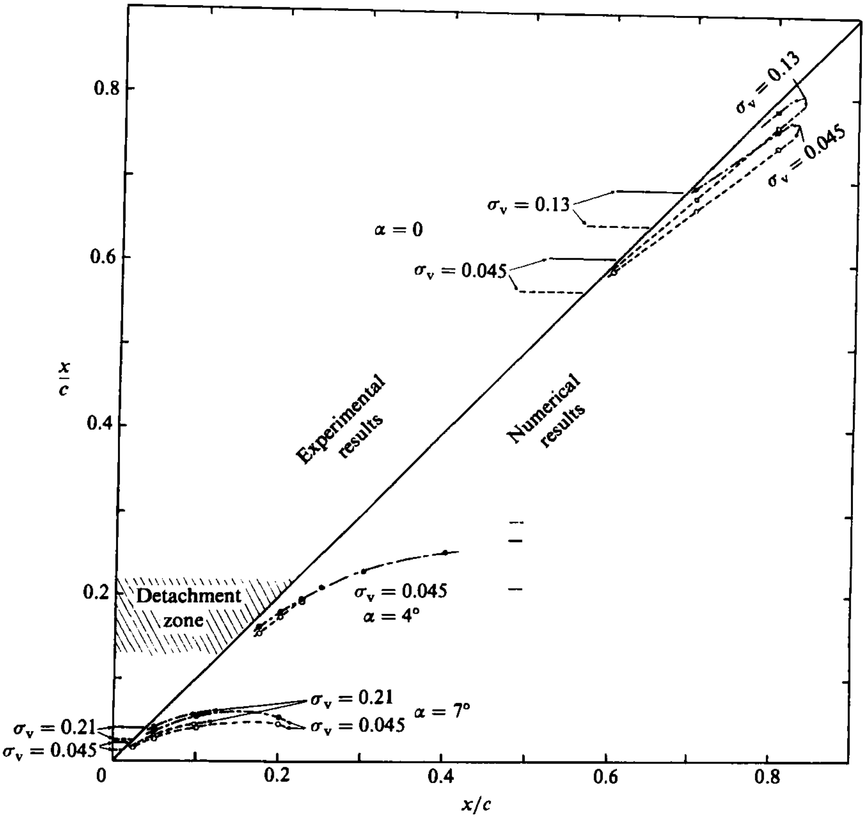

FIGURE 28. NACA 16012; abscissa of boundary layer characteristic points versus abscissa of cavity detachment under supercavitating conditions: -----, laminar separation; —-—, start of transition ($Re = 1000000$, $Tu = 1.15\%_0$); ——, cavity detachment.

In fact, there are two unknown detachment points: one on the upper side and one on the lower side. Here, the measured position of the lower-side detachment point is used for calculation, and only the upper-side detachment point is moved (except in the case $\alpha = 0$ for which both points are assumed to be located at the same unknown abscissa). Once the upper-side detachment is determined by the above criterion, it should be possible to determine the lower-side detachment by the same criterion, while the upper-side detachment is, in its turn, fixed at its calculated abscissa. If the calculated position of the lower-side detachment is different from the predicted position, the calculation has to be continued until convergence.

The calculated pressure-coefficient distribution, as well as the laminar boundary layer and the separation point, are independent of the Reynolds number. The only numerical result which actually depends on the Reynolds number is the transition point. This is in good agreement with experiments, which prove that the detachment point depends very little on the Reynolds number for slender bodies.

Figure 27 presents an example of numerical results obtained in the case $\alpha = 0$ and $\sigma_v = 0.045$. It shows that, when the detachment moves upstream from $x^+ = 8$ cm to $x^+ = 6$ cm (chord = 10 cm), the distance between separation and detachment decreases from about 6 mm to 1 mm. For $x^+ = 5$ cm, the computation predicts no separation. Thus, according to our criterion, the actual detachment point should take place in the neighbourhood of $x^+ = 6$ cm (which is the approximate detachment abscissa at which separation disappears). This prediction is in good agreement with the experiment. Figure 27 also shows that the corresponding calculated cavity length is about 30 % smaller than the experimental one.

Numerical results are shown in a more concise form and compared with experimental results in figure 28. The calculated abscissas of laminar separation and transition are plotted against the imposed abscissa of the cavity detachment. Experimental results are plotted on the left of the bisectrix and numerical results on the right. According to the proposed detachment criterion, the actual detachment should take place in the convergence domain of the bisectrix and the curve which gives laminar separation. It should not be overlooked that the boundary-layer calculation is stopped a little before the bisectrix in order to avoid the zone of influence of the streamwise pressure-gradient singularity. Figure 28 shows, for different cases of incidence and cavitation number, that prediction is in good agreement with experiment. The case of intermediate angles of attack appears different from that of low or high angles of attack. For $\alpha = 4°$, transition is very near to separation; if the detachment moves forward, calculations show that laminar separation may even disappear and, according to our criterion, no cavity can actually exist. This is in agreement with observations which show that the detachment is not two-dimensional along the span; on parts of the span, the cavity is glossy at detachment which indicates laminar separation just upstream, whereas, on some other parts, the cavity detaches much further behind and is wavy from the detachment point.

The effect of cavitation is to set a constant pressure-coefficient distribution level equal to $-\sigma_v$ behind the detachment. As a result, when the detachment moves forward, with all other conditions unchanged, the adverse-pressure-gradient zone becomes smaller. This explains why upstream of a given abscissa no laminar separation is predicted before detachment. A similar effect can be seen when the cavitation parameter is increased by decreasing the cavity length. The higher the value of σ_v, the lower the constant level $-\sigma_v$ of the pressure behind the detachment becomes, with corresponding reduction in importance of the adverse pressure gradient. Hence, there is a value of the cavitation parameter above which laminar separation disappears and consequently the cavity also disappears, according to our criterion. The computations show that, in the case $\alpha = 0$ and $x^+ = 7$ cm, laminar separation disappears for a value of σ_v between 0.13 and 0.19. This value is of the order of the cavitation inception parameter, which is found from experiments to be between 0.17 and 0.21.

The cavitating potential-flow model used here is a supercavitating model and is not therefore suitable for limited cavitation. Thus, it cannot give accurate predictions concerning cavitation inception. However, we believe that the proposed detachment criterion still holds true for limited cavitation under the condition that the cavitating-flow model is adequate for the degree of development of the cavity.

7. Conclusions

When a liquid contains only very small gas nuclei, it can withstand low pressures and even substantial tensions. Thus, on a curved wall along which a liquid flow is established, the cavitating zone can be preceded by a wetted region where pressure is lower than vapour pressure: the cavity detachment point is not the minimum pressure point. This assessment is substantiated by various experiments which show that the prominent factor governing the location of the cavity detachment is viscosity through the behaviour of the boundary layer: a largely developed cavity always detaches downstream of a laminar separation. In comparison, surface tension appears to have only a very local effect. Thus, the pressure-gradient distribution on the wetted region of a cavitating foil has two main functions. First, by integration from the reference point, it must lead to the vapour pressure at detachment. Secondly, it must control the boundary-layer development so that laminar separation takes place just upstream from detachment. In particular, an adverse pressure gradient is required in order to generate the laminar separation. This double condition is used to give a consistent description of the coexistence of boundary layer and developed cavitation: among all the pressure distributions which can be calculated on the basis of the potential-flow theory when varying the detachment point, only one is convenient from the boundary-layer viewpoint. The proposed criterion for the cavity detachment is in good agreement with experiments for various values of the liquid velocity U and the cavity relative underpressure σ which were obtained.

In the absence of laminar separation, unexpected results can be seen. For instance, when transition to turbulence takes place in the boundary layer after a change in the foil angle of attack, large cavities can disappear and the flow can become non-cavitating again. Moreover, developed cavitation may vanish as a result of the decrease in ambient pressure, the other parameters being kept constant: in this case, a further development of cavitation is not compatible with a laminar boundary layer, and a turbulent boundary layer is established in place of the cavity.

The general conclusion is that the strong connection between cavitation and laminar separation of the boundary layer on a curved wall, which was previously established by several investigators in the case of incipient cavitation, still holds for flows with largely developed cavities and supercavitating flows under the condition that the liquid has a sufficiently low gas nuclei content.

This research was supported for the most part by the French 'Direction des Recherches, Etudes et Techniques' (Contrats D.R.E.T. 80-414 and 81-513). We thank especially Mrs Biset who obtained the first results with elliptical cylinders.

REFERENCES

ACKERBERG, R. C. 1970 Boundary layer separation at a free streamline. Part 1. Two-dimensional flow. *J. Fluid Mech.* **44**, 211–225.

ACKERBERG, R. C. 1975 The effects of capillarity on free streamline separation. *J. Fluid Mech.* **70**, 333–352.

ALEXANDER, A. J. 1968 An investigation of the relationship between flow separation and cavitation. *N.P.L. Unpublished Report, Nov.* 1968.

ARAKERI, V. H. 1975 Viscous effects on the position of cavitation separation from smooth bodies. *J. Fluid Mech.* **68**, 779–799.

ARAKERI, V. H. & ACOSTA, A. J. 1973 Viscous effects in the inception of cavitation on axisymmetric bodies. *Trans. ASME* I: *J. Fluids Engng* **95**, 519–527.

ARMSTRONG, A. H. 1953 Abrupt and smooth separation in plane and axisymmetric flow. *Mem. Arm. Res. Est. G.B. No.* 22/53.

ARNAL, D., HABIBALLAH, M. & COUSTOLS, E. 1984 Théorie de l'instabilité laminaire et critère de transition en écoulement bi- et tri-dimensionnel. *Recherche Aérospatiale*, Vol. 1984–2.

BRENNEN, C. 1970 Cavity surface wave patterns and general appearance. *J. Fluid Mech.* **44**, 33–50.

DODU, J., DUPORT, J. & MICHEL, J. M. 1968 Le tunnel hydrodynamique de l'Université de Grenoble. *Houille Blanche* **7**, 697–702.

KNAPP, R. T., DAILY, J. W. & HAMMITT, F. G. 1970 *Cavitation*. McGraw-Hill.

Le Goff, J. P. & Lecoffre, Y. 1982 Nuclei and cavitation. In *Proc. of the 14th Symp. on Naval Hydrodynamics, Ann Arbor*, pp. 215–242. National Academy Press.

Michel, J. M. 1977 Wakes of developed cavitation. *J. Ship Res.* **21**, 225–238.

Michel, R. 1959 Critère de transition et amplification des ondes d'instabilité laminaire. *Recherche Aéronautique* **70**.

Oba, R., Ikohagi, T. & Yasu, S. 1980 Supercavitating cavity observations by means of laser velocimeter. *Trans. ASME* I: *J. Fluids Engng* **102**, 433–438.

Oldenziel, D. M. 1982 A new instrument in cavitation research: the cavitation susceptibility meter. *Trans ASME* I: *J. Fluids Engng* **104**, 136–142.

Pellone, C. & Rowe, A. 1981 Supercavitating hydrofoils in nonlinear theory. In *Proc. of the 3rd Intl Conf. on Numerical Ship Hydrodynamics, Paris*, pp. 399–412.

Rowe, A. & Michel, J. M. 1975 Two-dimensional base-vented hydrofoils near a free surface. Influence of the ventilation number. *Trans. ASME* I: *J. Fluids Engng* **97**, 465–474.

Schlichting, H. 1960 *Boundary Layer Theory*, 4th edn. McGraw-Hill.

Van der Meulen, J. H. J. 1978 A holographic study of the influence of boundary layer and surface characteristics on incipient and developed cavitation on axisymmetric bodies. In *Proc. of the 12th Symp. on Naval Hydrodynamics, Washington*, pp. 433–451. National Academy of Sciences.

Van der Meulen, J. H. J. 1980 Boundary layer and cavitation studies of Naca 16 012 and Naca 4412 hydrofoils. In *Proc. of the 13th Symp. on Naval Hydrodynamics, Tokyo*, pp. 195–219.

Van Dyke 1970 *Perturbation Methods in Fluid Mechanics*. Academic.

Villat, H. 1914 Sur la validité des solutions de certains problèmes d'hydrodynamique. *J. Math. Pures Appl.* **6**, 10.

Werle, H. 1980 Transition et décollement: visualisations au tunnel hydrodynamique de l'ONERA. *Recherche Aérospatiale* **5**, 331–345.

Wu, T. Y. T. 1972 Cavity and wake flows. *Ann Rev. Fluid Mech.* **4**, 243–284.